Li *et al. Micro & Nano Manufacturing* (2026) 2:7
https://doi.org/10.1007/s44374-026-00015-y

Micro & Nano Manufacturing

REVIEW Open Access

MEMS-enabled reconfigurable metasurface and nanophotonics: advances and perspectives

Dongxiao Li[1,2†], Weixin Liu[1,2†], Yinpeng Wang[1,2†], Daoye Zheng[1,2] and Chengkuo Lee[1,2*]

Abstract

Microelectromechanical systems (MEMS) have emerged as powerful technology for reconfigurable metasurface and nanophotonics, providing dynamic, low-power, and scalable control over optical functionalities that are inherently fixed in static nanophotonic devices. By introducing mechanical degrees of freedom, MEMS-enabled metasurface and nanophotonics allow real-time modulation of optical resonances, coupling strength, phase profiles, and radiation characteristics across a broad spectral range. This capability has opened new opportunities for adaptive sensing, tunable radiation sources, reconfigurable silicon photonic platforms, dynamic metalenses, and terahertz metasurfaces. In this Review, we present a comprehensive overview of recent advances in MEMS-enabled reconfigurable metasurface and nanophotonics, with a particular focus on application-driven developments in sensing, metasurface-based radiation sources, integrated silicon photonics, flat optics, and terahertz systems. Furthermore, we discuss emerging trends toward intelligent and programmable nanophotonic systems enabled by artificial intelligence–assisted design and closed-loop control. Finally, we outline the remaining challenges and future perspectives for translating MEMS-enabled reconfigurable nanophotonics from laboratory demonstrations to practical, large-scale applications.

Keywords microelectromechanical system (MEMS), reconfigurable metasurfaces, nanophotonics, adaptive optical sensing

Introduction

Nanophotonics has enabled unprecedented control over light–matter interactions by tailoring subwavelength structures to manipulate optical amplitude, phase, polarization, and spectral response [1–3]. Among them, metasurfaces, photonic crystals, plasmonic nanoantennas, and integrated photonic circuits have led to transformative advances in sensing [4, 5], imaging [6–8], communications [9], and on-chip information processing [10]. However, most nanophotonic devices remain inherently static, with their functionality fixed once fabricated, which fundamentally limits adaptability to dynamic environments, multifunctional operation, and system-level optimization. To overcome these limitations,

†Dongxiao Li, Weixin Liu and Yinpeng Wang contributed equally to this work.

*Correspondence:
Chengkuo Lee
elelc@nus.edu.sg
[1]Department of Electrical and Computer Engineering, National University of Singapore, 117583 Singapore, Singapore
[2]Center for Intelligent Sensors and MEMS, National University of Singapore, 117608 Singapore, Singapore

reconfigurable nanophotonics has emerged as a critical research direction, aiming to dynamically tune optical responses in real time [11].

Various tuning mechanisms have been explored, including thermo-optic effects [12], phase-change materials [13–15], carrier injection or depletion in semiconductor platforms [16, 17], and two-dimensional materials [18, 19]. These approaches primarily rely on modulating the intrinsic material properties of photonic structures, typically through refractive index changes induced by thermal, electrical, or phase transitions. While such strategies have enabled partial tunability, they often involve intrinsic trade-offs, including high power consumption, limited tuning range, slow response speed, optical loss, or material fatigue. Conceptually, these material-property-based approaches represent one class of tuning paradigm in reconfigurable nanophotonics. In contrast, microelectromechanical systems (MEMS) introduce a fundamentally different strategy by enabling direct modulation of device geometry and coupling topology. A comparison of representative tuning mechanisms used in reconfigurable nanophotonics, including their tuning range, response speed, power consumption, optical loss, scalability, and typical applications, is summarized in Table 1. Instead of slightly perturbing refractive indices, MEMS actuation mechanically reconfigures key structural parameters that govern light-matter interactions at the nanoscale, including gap spacing, relative alignment, resonant cavity length, and coupling distance. Because nanophotonic responses are highly sensitive to subwavelength geometry, even small mechanical displacements can induce large and reversible changes in optical resonance, field confinement, and radiation properties. This geometry-driven tuning mechanism forms a unifying principle of MEMS-enabled reconfigurable nanophotonics and enables a level of optical reconfigurability that is difficult to achieve through material tuning alone.

MEMS-enabled reconfigurable nanophotonics threrfore leverages mechanical motion to modulate key photonic parameters such as gap spacing, coupling strength, resonant conditions, and radiation patterns [20–26]. By introducing an additional mechanical degree of freedom, MEMS allows nanophotonic structures to transition from static optical elements to dynamically tunable and even programmable systems. This paradigm has led to a wide range of reconfigurable devices, including tunable metasurfaces for beam steering and spectral control, adaptive nanophotonic sensors with enhanced sensitivity and selectivity, MEMS-integrated thermal and terahertz radiation sources, reconfigurable silicon photonic platforms, and mechanically tunable metalenses for adaptive imaging.

In recent years, the convergence of MEMS technology with metasurfaces, silicon photonics, and terahertz nanophotonics has significantly expanded both the functionality and the application space of reconfigurable photonic systems (Fig. 1). Importantly, advances in large-area MEMS actuation, CMOS-compatible fabrication, and heterogeneous integration have enabled scalable and system-level implementations, moving MEMS-enabled nanophotonics beyond proof-of-concept demonstrations toward practical deployment. At the same time, the growing complexity of reconfigurable nanophotonic systems has motivated the adoption of artificial intelligence (AI) and machine learning techniques for device design, optimization, and control [27, 28]. AI-assisted inverse design, physics-informed neural networks, and closed-loop optimization strategies have shown great promise in navigating the high-dimensional design space of MEMS–nanophotonic systems and in enabling adaptive, self-optimized operation. These developments are driving a transition from reconfigurable to programmable and intelligent nanophotonics, where photonic functionality can be dynamically adapted in response to environmental feedback and application demands.

Although several excellent reviews have addressed either reconfigurable metasurfaces, optical MEMS, or tunable nanophotonic devices, a comprehensive

Table 1 Comparison of major tuning mechanisms in reconfigurable photonic devices

Mechanism	Working wavelength	Speed/ Voltage	Tuning Range	Power consumption	Optical loss	Scalability	Applications
Thermo-optic	Vis–MIR	µs–ms / ~1–10 V	Moderate	High	Low–moderate	Limited by thermal crosstalk	modulators, filters, phase shifters, beam steering
Phase-change materials	Vis–MIR	ns–µs / ~1–5 V	Large	Moderate–high	Moderate–high	Limited cycling endurance	switches, filters, memory, programmable photonic circuits
2D materials	Vis–MIR	ps–ns / 1–20 V	Small–moderate	Low	Moderate	Integration still developing	modulators, photodetectors
Carrier injection / depletion	NIR	ps–ns / ~1–5 V	Small	Moderate	moderate	Excellent CMOS compatibility	modulators, phase shifters, switches
MEMS	Vis–THz	Tens ns–ms / ~1–100 V	Large	Very low	low	CMOS compatible but complex process	Switches, filters, beam steering, tunable lenses, sensors

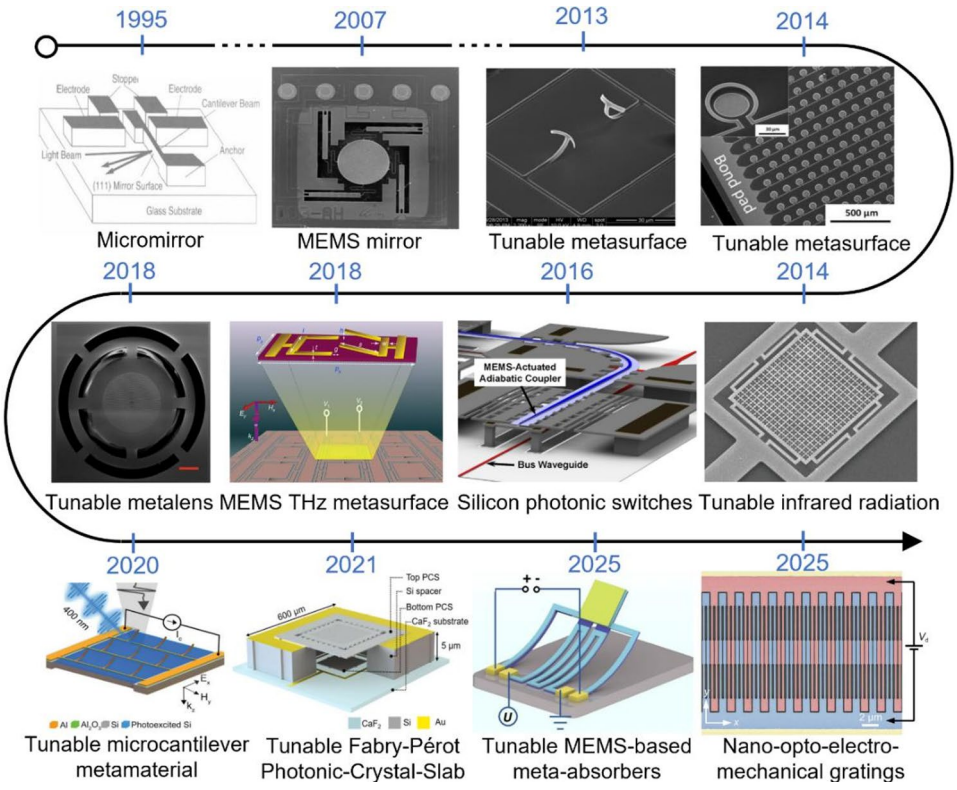

Fig. 1 Roadmap of MEMS-enabled reconfigurable nanophotonics. Reproduced with permission [23]. Copyright 1995, IOP Publishing. Reproduced with permission [29]. Copyright 2007, IOP Publishing. Reproduced with permission [30]. Copyright 2013, AIP Publishing. Reproduced with permission [24]. Copyright 2014, AIP Publishing. Reproduced with permission [31]. Copyright 2014, Wiley. Reproduced with permission [32]. Reproduced with permission [33]. Copyright 2016, Optica Publishing Group. Copyright 2018, Springer Nature. Reproduced with permission [34]. Copyright 2018, Springer Nature. Reproduced with permission [35]. Copyright 2020, Wiley. Reproduced with permission [36]. Copyright 2021, Elsevier. Reproduced with permission [37]. Copyright 2025, Springer Nature. Reproduced with permission [17]. Copyright 2025, AAAS

perspective that systematically integrates MEMS-enabled reconfigurable metasurface and nanophotonics across applications, platforms, and emerging intelligent design paradigms remains lacking. In this Review, we provide a structured overview of recent advances in MEMS-enabled reconfigurable metasurface and nanophotonics, with a particular focus on sensing, radiation sources, silicon photonic platforms, metalenses, and terahertz metasurfaces. Furthermore, we highlight the role of AI-assisted design and intelligent control in shaping the next generation of programmable nanophotonic systems and discuss key challenges and future opportunities for this rapidly evolving field.

MEMS actuation mechanisms for reconfigurable nanophotonics

Microelectromechanical systems (MEMS) provide an effective platform for dynamically tuning nanophotonic structures by converting electrical stimuli into controlled mechanical motion [38,]39]. Unlike material-property-based tuning approaches that rely on refractive index modulation, MEMS actuation directly modifies the geometry and relative positioning of photonic components. Because the optical response of metasurfaces and nanophotonic structures is highly sensitive to subwavelength structural variations, even small mechanical displacements can induce significant changes in resonance frequency, phase, amplitude, and radiation characteristics [34].

Depending on the direction of mechanical displacement, MEMS actuation schemes can generally be categorized into out-of-plane (vertical) [40] and in-plane (lateral) motion [41]. Out-of-plane actuation typically modifies the air gap between metasurface elements and the substrate or between stacked photonic structures, thereby enabling dynamic tuning of resonant conditions and field confinement. In contrast, in-plane actuation adjusts the lateral position, alignment, or coupling distance between nanophotonic elements, which can be used to control near-field coupling, phase gradients, or radiation patterns. These two actuation modes provide complementary strategies for reconfiguring nanophotonic devices.

Various actuation mechanisms have been developed to generate such mechanical motion in MEMS-enabled photonic systems [42–45]. Among them, electrothermal,

Table 2 Comparison of common MEMS actuation mechanisms for nanophotonics

Actuation Mechanism	Displacement	Response Speed	Driving Voltage	Power Consumption	CMOS Compatibility
Electrothermal	Large (> 1 μm)	Slow (ms)	Low (< 10 V)	High (Steady-state)	Excellent
Electrostatic	Moderate (< 1 μm)	Fast (μs)	High (1–100 V)	Very Low	Excellent
Piezoelectric	Small/Moderate	Very Fast (ns-μs)	Moderate	Low	MaterialDependent

electrostatic, and piezoelectric actuation are the most widely used due to their compatibility with microfabrication technologies and their ability to provide controllable displacement at the microscale. Each mechanism offers distinct trade-offs in driving voltage, response speed, displacement range, and power consumption (Table 2). Their fundamental operating principles are briefly discussed in the following sections.

Electrothermal actuation

Electrothermal actuation is one of the most widely adopted MEMS tuning mechanisms for metasurfaces [46], as it enables relatively large mechanical displacement under modest driving voltages and can be readily

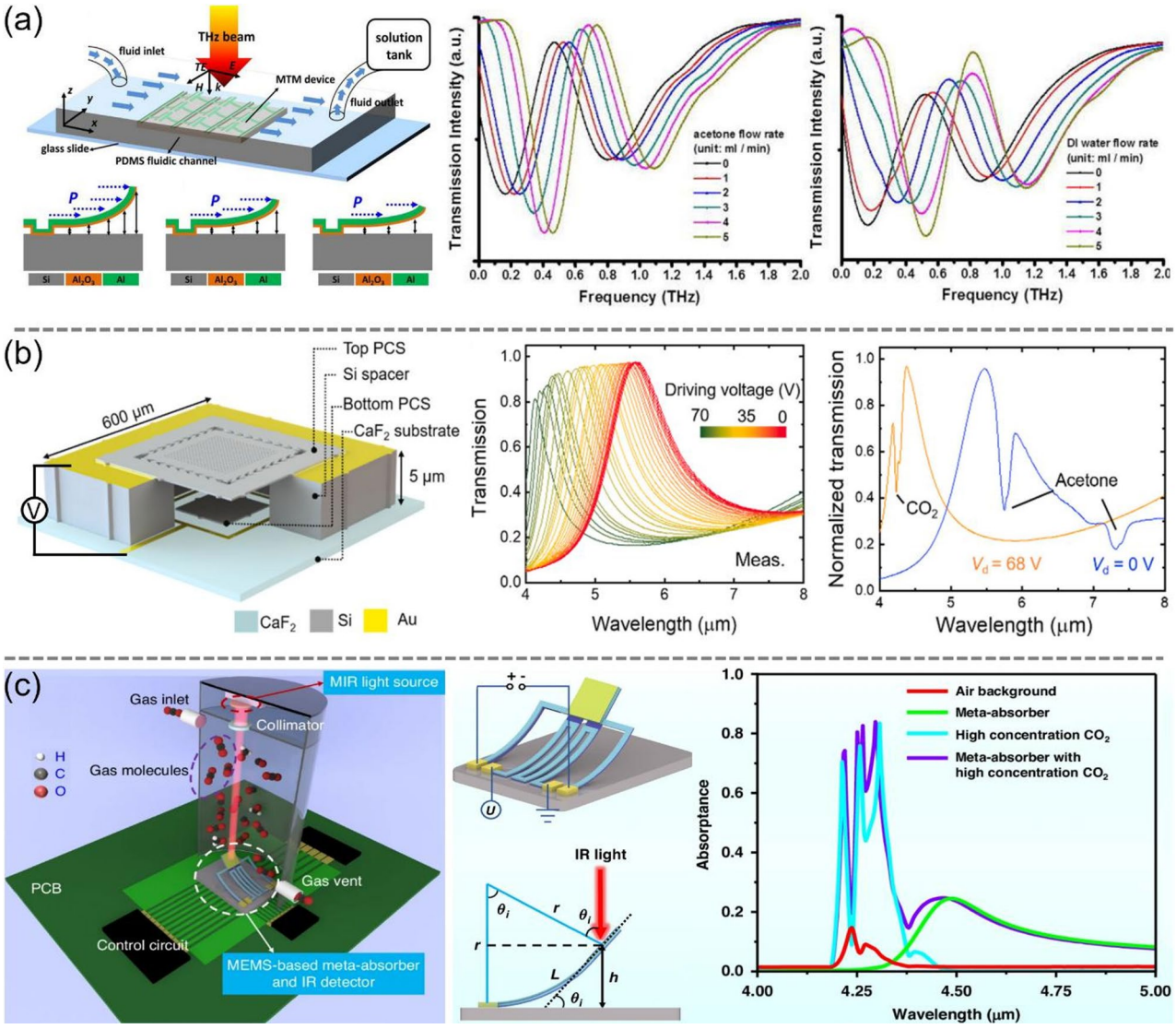

Fig. 2 MEMS-Enabled Nanophotonics for Sensing. **a** Tuning characteristics of mirrorlike T-shape terahertz metamaterial using out-of-plane actuated cantilevers. Reproduced with permission [81]. Copyright 2014, AIP Publishing. **b** Tunable Fabry-Pérot photonic-crystal-slab filter towards wearable mid-infrared computational spectrometer. Reproduced with permission [36]. Copyright 2021, Elsevier. **c** Tunable MEMS-based meta-absorbers for nondispersive infrared gas sensing applications. Reproduced with permission [37]. Copyright 2025, Springer Nature

implemented using CMOS-compatible material stacks. In a typical electrothermal metasurface, an injected current generates Joule heating in an integrated resistive path, producing a temperature rise in a suspended bimorph cantilever. Due to the mismatch in the coefficients of thermal expansion (CTE) between the two layers, the resulting thermal strain is converted into a bending moment that causes controllable mechanical deformation of the structure [47].

The resulting vertical displacement can be estimated using a simplified bilayer beam model. For a canonical bilayer cantilever, the tip-to-substrate vertical displacement δ can be approximated as [47, 49]

$$\delta = \frac{3W_1W_2E_1E_2t_1t_2(t_1+t_2)(\alpha_2-\alpha_1)\Delta T \cdot L^2}{(E_1W_1t_1^2)^2 + (E_2W_2t_2^2)^2 + 2W_1W_2E_1E_2t_1t_2(2t_1^2+3t_1t_2+2t_2^2)} \quad (1)$$

where W, t, and L denote the cantilever width, thickness, and length, respectively; E and α represent the Young's modulus and CTE of each layer; and ΔT is the temperature increase induced by resistive heating. This relationship highlights several key design dependencies: the displacement scales approximately with L^2 and with the CTE mismatch (α_2-α_1), while also being influenced by the composite bending stiffness of the layered structure. Consequently, material pairs with large CTE mismatch and appropriately designed cantilever geometries are often employed to enhance the achievable displacement.

Electrothermal actuators typically operate at driving voltages of a few volts and can generate relatively large mechanical displacement, making them particularly suitable for metasurface tuning applications. In nanophotonic systems, this mechanism has been widely used to achieve full 2π phase modulation or wide-range resonance frequency shifting by dynamically modifying structural parameters such as air gaps, resonator alignment, or coupling distances. However, the modulation bandwidth is generally limited by the thermal time constant of the structure, with response times typically ranging from microseconds to milliseconds. In addition, continuous electrical power is required to maintain the temperature gradient, which may lead to increased power consumption and potential thermal crosstalk in densely integrated metasurface arrays.

In addition to out-of-plane bending configurations, electrothermal actuation can also be implemented for in-plane mechanical motion [50]. In such designs, thermal expansion of microbeams or specially engineered actuator geometries (e.g., V-shaped or chevron actuators) generates lateral displacement that translates suspended metasurface elements or photonic components. This in-plane actuation mechanism is widely used to dynamically tune the relative position, coupling distance, or overlap between nanophotonic structures. Compared with out-of-plane bimorph bending, in-plane electrothermal actuators often provide larger lateral forces and are well suited for applications requiring precise alignment or controllable near-field coupling in reconfigurable nanophotonic systems.

Electrostatic actuation

Electrostatic actuation is widely used in MEMS-enabled reconfigurable metasurfaces due to its low static power consumption, fast response, and straightforward electrical addressing [48]. In this mechanism, a voltage applied between a suspended cantilever (or membrane) and an underlying electrode generates an electrostatic field across the air gap, producing a voltage-dependent attractive force that competes with the mechanical restoring force of the structure.

For a simplified parallel-plate actuator, the electrostatic force can be expressed as [48].

$$F_{es} = \frac{1}{2}\frac{\varepsilon_0 A V^2}{(g-x)^2} \quad (2)$$

where ε_0 is the vacuum permittivity, A is the electrode overlap area, V is the applied voltage, g is the initial gap, and x is the displacement of the movable structure. The restoring force of the compliant structure can be approximated as F_m=kx, where k is the effective spring constant. When the electrostatic force exceeds the restoring force, the movable structure becomes unstable and collapses onto the substrate, a phenomenon known as pull-in [51]. For a parallel-plate actuator, pull-in typically occurs when the displacement reaches approximately one-third of the initial gap. Operation below the pull-in voltage allows continuous analog tuning of optical responses, whereas pull-in can be exploited for high-contrast switching between discrete mechanical states.

Electrostatic actuators typically operate at driving voltages ranging from a few volts to several tens of volts, depending on the actuator geometry and electrode gap, and can exhibit fast response times from microseconds to sub-microseconds, making them well suited for high-speed optical modulation. This actuation mechanism can be implemented in both out-of-plane configurations (cantilever or membrane bending, modulating vertical gaps) and in-plane configurations (comb-drive or lateral actuators, tuning relative positions or coupling distances), providing flexible strategies for dynamically reconfiguring nanophotonic structures. Overall, electrostatic actuation provides high-speed operation and low static power consumption, but requires careful design to avoid pull-in instability, and the maximum achievable displacement is generally smaller than that of electrothermal actuators. Its compact form factor and CMOS compatibility make it

widely adopted in tunable metasurfaces, optical switches, and reconfigurable photonic circuits.

Piezoelectric actuation

Piezoelectric actuation provides an efficient electromechanical transduction mechanism for MEMS-enabled reconfigurable nanophotonic systems by converting an applied electric field directly into mechanical strain through the converse piezoelectric effect [48, 52, 53]. Compared with electrothermal and electrostatic actuation, piezoelectric actuators can offer fast response and low static power consumption, making them attractive for high-speed tunable photonic devices.

In a typical piezoelectrically driven metasurface, a piezoelectric thin film (such as PZT or AlN) is integrated with a passive elastic layer to form a unimorph or bimorph actuator [54]. When a voltage is applied across the piezoelectric layer, an in-plane strain is generated due to the converse piezoelectric effect. The mismatch in strain between the active piezoelectric layer and the passive elastic layer produces a bending moment that deflects a suspended cantilever or membrane. This mechanical deformation modifies key structural parameters of the nanophotonic unit cell, such as the air gap, overlap area, or effective current path, which can be interpreted as a change in the equivalent capacitance or inductance of the metasurface element. As a result, the resonance frequency, phase response, and amplitude characteristics can be dynamically tuned.

For a piezoelectric bilayer cantilever with one end clamped, the application of an external voltage V across the piezoelectric layer induces an in-plane actuation strain that bends the composite beam and produces an out-of-plane displacement at the free end. According to a simplified bilayer beam model, the tip displacement can be approximated as [49, 55].

$$\delta_{tip} = \frac{L^2 d_{31} V / t_p (t_p + t_e) A_p E_p A_e E_e}{4(E_p I_p + E_e I_e)(A_p E_p + A_e E_e) + (A_p E_p A_e E_e)(t_p + t_e)^2} \quad (3)$$

where L is the cantilever length, d_{31} is the transverse piezoelectric coefficient, t_p and t_e are the thicknesses of the piezoelectric and elastic layers, A_p and A_e are the corresponding cross-sectional areas, E_p and E_e denote the Young's moduli, and I_p and I_e represent the second moments of area of the two layers.

Piezoelectric actuators typically operate at driving voltages of a few volts to tens of volts and exhibit fast response times ranging from nanoseconds to microseconds, depending on the device geometry and mechanical resonance frequency. Similar to other MEMS actuators, piezoelectric actuation can be implemented in both out-of-plane bending configurations and in-plane displacement structures, enabling either vertical gap modulation or lateral tuning of coupling between nanophotonic elements.

Overall, piezoelectric actuation provides fast response, relatively low power consumption, and precise displacement control. However, the achievable displacement is typically smaller than that of electrothermal actuators, and integration of high-performance piezoelectric materials may introduce additional fabrication complexity. Despite these challenges, piezoelectric MEMS actuators have been widely explored for tunable metasurfaces, optical switches, adaptive lenses, and reconfigurable photonic circuits.

Applications of MEMS-enabled reconfigurable metasurface and nanophotonics

MEMS-enabled nanophotonics for sensing

Static nanophotonic structures, including plasmonic nanoantennas, photonic crystals, and metasurfaces, have enabled remarkable advances in optical sensing by providing strong field confinement and enhanced light–matter interactions at subwavelength scales [10],[56–61]. In particular, static metasurface-based sensors have demonstrated high sensitivity and molecular selectivity across the terahertz (THz) and mid-infrared (MIR) spectral regions, exploiting engineered resonances to amplify the interaction with vibrational and rotational molecular fingerprints [7, 62–73]. Such approaches have been widely explored for chemical and biological sensing. Carefully designed resonant modes, such as localized surface plasmon resonances [74–76], guided-mode resonances [77], and bound states in the continuum [5, 78–80], enable the detection of minute refractive index changes or absorption signatures.

Despite these successes, static nanophotonic and metasurface sensors are inherently limited by their fixed spectral responses, which are determined at the fabrication stage. Any deviation arising from fabrication tolerances, environmental fluctuations, or variations in target analytes can lead to spectral mismatch, degraded sensitivity, or the need for multiple devices to cover different sensing targets. Moreover, broadband or multi-species sensing using static metasurfaces typically requires either large device arrays or external spectroscopic components, which increases system complexity and power consumption. These fundamental limitations have motivated the development of dynamic and adaptive sensing strategies, where the optical response of nanophotonic structures can be actively tuned to match the spectral characteristics of target analytes in real time. In this context, MEMS-enabled reconfigurable nanophotonics offers a compelling solution. By mechanically modulating optical resonances, coupling conditions, or effective cavity lengths, MEMS-based nanophotonic sensors can dynamically align spectral responses with molecular absorption

features, enhance light–matter interaction, and improve robustness against environmental fluctuations. This capability is particularly critical in the THz and MIR spectral regions, where molecular fingerprinting relies on precise spectral matching.

Early demonstrations of MEMS-enabled reconfigurable sensing can be found in the THz regime, where mechanically tunable metastructures provide effective control over resonant characteristics. For example, Lin et al. proposed integrating a mirror-symmetric T-shaped terahertz metamaterial with an out-of-plane actuated MEMS cantilever to achieve dynamic tuning of its electromagnetic response (Fig. 2a) [81]. The resonant frequency of the device can be actively modulated via electrostatic actuation or liquid-induced forces, yielding a tuning range of up to 0.50 THz. Notably, a liquid-based modulation scheme was demonstrated, in which covering the device with deionized water induced resonance shifts of 0.17 THz and 0.21 THz for the inductive-capacitive and dipolar modes, respectively. This work clearly illustrates how out-of-plane MEMS actuation enables large tuning ranges without introducing additional optical loss, making it particularly attractive for THz sensing applications where conventional material-based tuning mechanisms are limited. The mechanically induced resonance shift provides a direct pathway for adaptive THz spectroscopy and sensing of materials with frequency-dependent absorption features.

Building upon mechanically tunable resonant structures, MEMS-enabled nanophotonics has further evolved toward system-level spectroscopic sensing platforms in the mid-infrared. Chang et al. developed a triboelectrically tunable Fabry–Pérot filter based on a photonic crystal slab, serving as the core component of a wearable MIR computational spectrometer (Fig. 2b) [36]. In this approach, MEMS actuation dynamically modulates the cavity spacing of the Fabry–Pérot filter, enabling wavelength-selective transmission across the MIR fingerprint region. Notably, the integration of a triboelectric energy-harvesting mechanism allows self-powered operation, highlighting the synergy between MEMS actuation, nanophotonic filtering, and wearable sensing systems. Furthermore, by identifying molecular fingerprints, the authors reconstructed the transmission spectra of CO2 and acetone. This work demonstrates how combining reconfigurable nanophotonic filters with computational reconstruction can substantially reduce system complexity, paving the way for compact, low-power wearable MIR sensing platforms without reliance on bulky static broadband spectrometers.

More application-oriented implementations of MEMS-enabled nanophotonics have been realized in gas sensing, where selective absorption in the infrared provides a robust detection mechanism. Li et al. developed a tunable MEMS-based superabsorber for non-dispersive infrared (NDIR) gas sensing (Fig. 2c) [37]. The proposed superabsorber exhibits angle-dependent resonant behavior, enabling spectral matching to the absorption features of different gases by varying the incidence angle of the illumination. Compared with conventional fixed-wavelength NDIR systems, this sensor demonstrates enhanced tunability and selectivity. The MEMS-enabled tunability allows a single device to adaptively address different gas species or compensate for fabrication-induced resonance offsets, which is a long-standing challenge in practical gas sensor deployment. Furthermore, the authors conducted a preliminary investigation of the sensing performance for CO2 detection. This work exemplifies how MEMS-reconfigurable metasurfaces can bridge the gap between laboratory-scale nanophotonic devices and real-world sensing applications, offering a scalable and robust solution for environmental and industrial monitoring.

In summary, these studies demonstrate the versatility of MEMS-enabled nanophotonics for sensing across the THz and infrared spectral ranges. From fundamental resonance tuning using out-of-plane actuation, to wearable computational spectroscopy, and finally to application-ready gas sensing platforms, MEMS provides a unifying mechanical tuning framework that enhances adaptability, spectral precision, and system robustness. These advantages position MEMS-enabled reconfigurable nanophotonics as a key technology for next-generation intelligent and adaptive sensing systems.

MEMS-enabled reconfigurable silicon photonic platforms

Silicon photonics has emerged as an important platform for integrated optics, largely because it supports compact devices and can be fabricated with processes compatible with CMOS technology. Yet in many applications, guiding light on chip is only part of the challenge. The circuit must also be tunable. In practice, the response of silicon photonic devices often shifts because of fabrication imperfections, temperature changes, or operating-wavelength variations. As circuits become more complex, this sensitivity makes post-fabrication adjustment increasingly important. Tunability allows designers to correct phase errors, rebalance coupling, align resonances, and reconfigure signal paths when needed. Without it, the function of a photonic circuit would be largely fixed at the time of fabrication, leaving little room for adaptation or large-scale programmability.

Integrating MEMS actuators with nanophotonic waveguides has therefore become one of the most compelling routes to practical reconfigurability in integrated optics, mainly because it addresses two key bottlenecks in large-scale waveguide systems: (i) the limited tuning range of individual elements and (ii) the power and the thermal overhead that scales unfavorably with circuit

size. Conventional silicon photonics have relied heavily on thermo-optic tuning and free-carrier effects [82–84]. These approaches are attractive for their process simplicity, but the induced refractive-index perturbation is relatively small and often accompanied by penalties such as static power dissipation, thermal crosstalk, added optical loss, or wavelength sensitivity. These drawbacks become especially problematic when hundreds to thousands of tuning elements are required [85–87]. In contrast, instead of slightly changing the material index, MEMS enables direct geometric reconfiguration of the waveguide configuration, including the gap, overlap, or symmetry, thereby producing large optical changes with near-zero standby power.

A landmark example that established this scaling argument is the large-port-count silicon photonic crossbar switch enabled by MEMS-actuated vertical couplers, representative of Fig. 3a [33]. In this architecture, switching is implemented in a digital manner that each coupler is driven between strongly coupled and effectively decoupled states, so that the signal experiences a well-defined routing element rather than accumulating analog phase errors across many biased interferometers. This approach enabled a 64 × 64 crossbar switch with broadband behavior, illustrating how mechanically switching coupling topology can circumvent the bandwidth and footprint trade-offs inherent to ring-resonator switches or the loss accumulation typical of long cascaded MZI meshes. It indicates that MEMS allows routing fabrics to scale toward very large port counts because the optical penalty is tied to the number of traversed switching cells rather than the total number of elements present on chip.

More recently, the field has shifted from demonstrating isolated MEMS switches to building programmable waveguide systems where many tunable couplers and phase shifters operate together, as shown conceptually by Fig. 3b [88]. In this work, tunable directional couplers are realized by mechanically adjusting waveguide separation to directly control evanescent coupling, and phase shifters are implemented via gap-dependent perturbation of the effective index. It provides very low standby power (< 10 fW), low programming voltages (< 11 V), sub-decibel optical loss, and > 30 dB extinction in continuously tunable couplers, which collectively point to a credible path for scaling programmable photonic integrated circuits without thermal management becoming the dominant system constraint.

MEMS-tunable waveguide concepts are also proving particularly natural in spectral regions where conventional silicon photonics have fewer mature tuning options [89–91]. Qiao and co-workers demonstrated a multifunctional photonic switch operating in the mid-infrared range (3.8–4.0 μm) using a MEMS-based tunable coupler in a suspended subwavelength-grating (SWG) waveguide platform, with flip-chip bonding used to enable a double-layer configuration and a larger air gap for electrostatic actuation (Fig. 3c) [89]. For mid-IR waveguides that have larger-mode and are more sensitive to material absorption, mechanical tuning is appealing because it can strongly modulate coupling without introducing the free-carrier absorption penalties that are severe at longer wavelengths, and without requiring high continuous heating power. More broadly, suspended and undercut waveguides that commonly used in mid-IR to reduce substrate leakage are structurally compatible with MEMS release steps [92, 93], suggesting a practical synergy between mid-IR nanophotonics and MEMS manufacturing workflows.

Another direction where MEMS tuning is not merely convenient but arguably enabling is mode control in multimode waveguides, represented by Fig. 3d [94]. Mode-division multiplexing and higher-order mode processing demand devices that can selectively couple between modes while keeping crosstalk low. In the MEMS-enabled programmable mode switch, vertical comb-drive actuation is used to change the coupling condition between tailored waveguide sections, enabling controllable redistribution among TE0/TE1/TE2 channels. A particularly relevant system-level point is the very low static power needed to hold a coupled state (~ tens of pW, dominated by leakage), demonstrating again the set-and-hold advantage of electrostatic MEMS. Mechanically, these devices still operate in the microsecond regime (tens of μs), which is slower than electro-optic modulation but entirely adequate for reconfigurable routing, adaptive mode management, or system reprogramming.

More recently, mechanical reconfiguration has enabled optical functions that are difficult to obtain with conventional waveguide tuning, exemplified by pixelated nano-opto-electro-mechanical (NOEM) gratings for programmable spectral shaping (Fig. 3e) [17]. In this work, Liu et al. discretized a Bragg grating into independently biased pixels and exploited electromechanically induced symmetry breaking to locally control the coupling strength, enabling programmable longitudinal coupling profiles and thus reconfigurable spectral responses in an ultracompact footprint (~ 0.007 mm^2). The results further indicate that NEMS-scale actuation can support nanosecond-class wavelength-selective switching with very high contrast, providing a promising route toward compact, rapidly reconfigurable on-chip spectral processors without the large footprint.

Taken together, recent developments highlight MEMS as a geometry-driven tuning approach with large optical leverage and near-zero standby power, directly addressing the scaling constraints of thermal tuning in dense waveguide systems. At the same time, widespread deployment

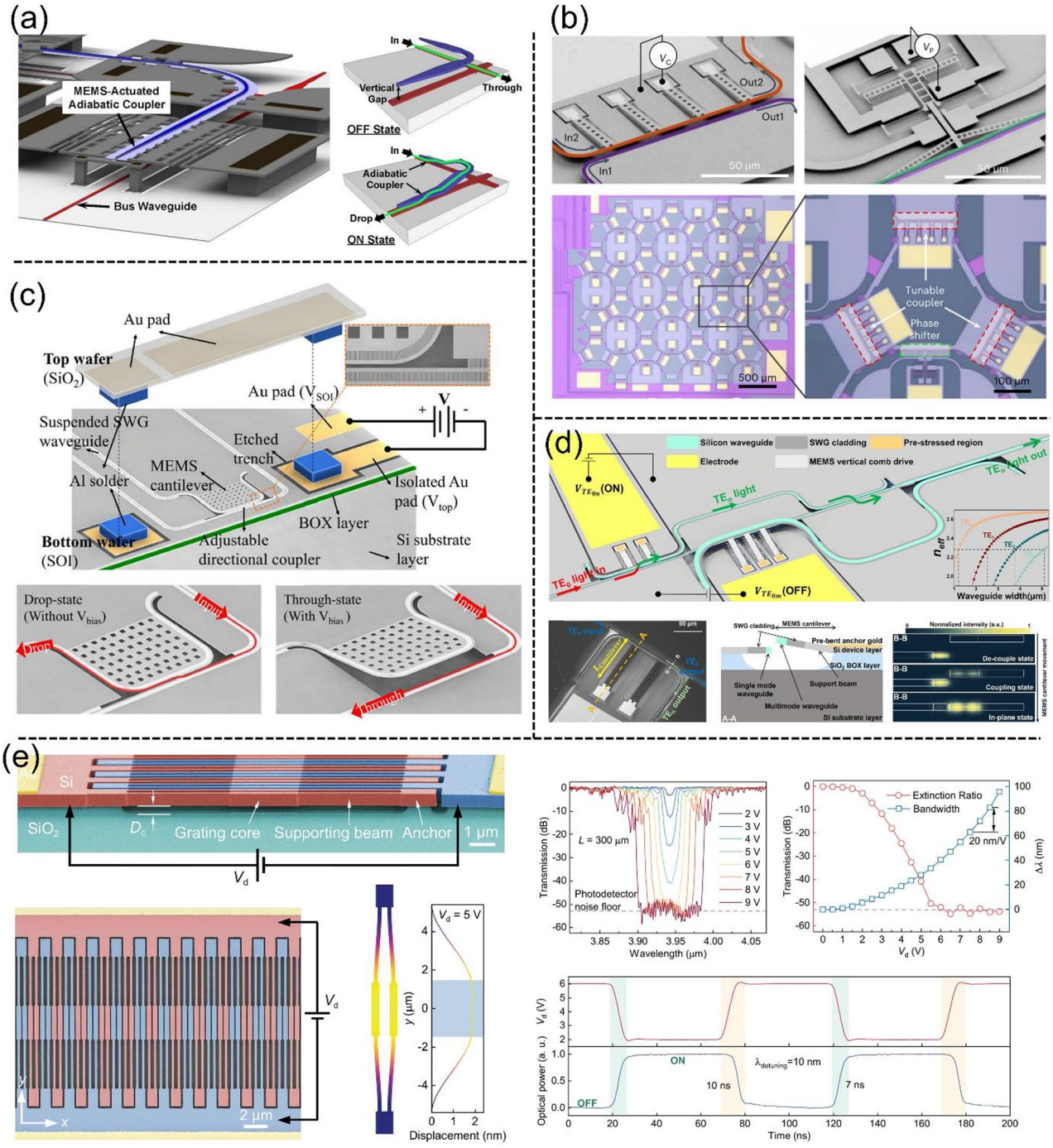

Fig. 3 MEMS-tunable nanophotonic waveguide devices enabling reconfigurable optical functions. **a** Large-port-count broadband silicon photonic switch using MEMS-actuated vertical couplers. Reproduced with permission [33]. Copyright 2016, Optica Publishing Group. **b** Programmable photonic circuit elements (tunable couplers and phase shifters) based on electrostatic MEMS waveguide actuation. Reproduced with permission [88]. Copyright 2023, Springer Nature. **c** Mid-infrared multifunctional switch using a MEMS-tunable suspended-waveguide coupler. Reproduced with permission [89]. Copyright 2020, Optica Publishing Group. **d** MEMS-enabled mode switching via tunable mode converters for multimode waveguides. Reproduced with permission [94]. Copyright 2024, Wiley. **e** Pixelated nano-opto-electro-mechanical grating for ultracompact, programmable spectral shaping. Reproduced with permission [17]. Copyright 2025, AAAS

will depend on manufacturability and reliability, including stiction control in released structures, mitigation of dielectric charging and drift, and practical driver/packaging co-design (e.g., wafer-level encapsulation and heterogeneous electronic integration) [85, 95, 96]. As integrated photonics continues to evolve toward dense, reconfigurable waveguide systems, MEMS provides a technically grounded pathway to maintain programmability while controlling system-level power, crosstalk, and loss.

MEMS vertical actuation platform for tunable metamaterials

As a typical MEMS-driven platform, the vertically actuated structure provides a simple and effective way to mechanically reconfigure micro-devices. It relies on a suspended element that can be moved toward a fixed electrode under an applied voltage, allowing controlled and repeatable out-of-plane motion. The vertical actuation is compact, energy-efficient, and CMOS compatible, making it widely used for tunable metamaterials to flexibly manipulate light field.

In its early development, the vertical actuation platform mainly relied on pull-in induced state switching. This mechanism is well compatible to the classical metal-dielectric-metal (MIM) configuration [97, 98]. When the applied voltage reached a critical level, the suspended metasurface collapsed onto the ground plane, producing a transition between two optical states. Using this mechanism, in 2013, Liu et al. demonstrated a MEMS metamaterial absorber that toggles between reflective and highly absorbing states through snap-down actuation, establishing a simple but effective method for distinct optical mode switching (Fig. 4a) [31]. Subsequently, they applied the same mechanism to a MEMS thermal emitter, demonstrating the switchable thermal emission without the need to change temperature (Fig. 4b) [99]. However, there are still some shortcomings such as uneven displacement of different positions and only two controllable states. Then, the vertical actuation platform evolves from binary switching to continuous tuning. Instead of relying on pull-in collapse, the air gap can be gradually adjusted to continuously shift resonance wavelengths. In Fig. 4c, Wang et al. designed a tunable high-Q infrared absorber by tuning the distance between free-standing all-metallic metasurface layer and suspended metallic mirror layer that is attracted by bottom electrodes [100]. The moveable metallic mirror and free-standing layer form a tunable Fabry–Pérot cavity, which enables wide-range narrowband absorption tuning from 8.5 to 14 μm. Then, Wang et al. proposed an optimized design shown in Fig. 4d, the suspended metallic metasurface layer is configurated with Si frames that are attracted by electrostatic force, which avoids the inhomogeneous displacements and deformation at different positions of the freestanding layer [101]. With a buried resistance heater, the wavelength of radiated infrared emission can be varied from 9.62 to 7.94 μm. In addition, dielectric metamaterial can also integrate with this platform. In Fig. 4e, Chang et al. proposed a dual-layer Si metasurface with tunable transmission peak that can be tuned by using electrostatic force to change the distance between two layers [36]. Then, this device is applied as a computational spectrometer for gas sensing applications. Furthermore, the vertical actuation platform can also make the device layer tilted. In 2019, Hosteen et al. developed a Si metasurface for dynamic beam shaping and color mixing, by controlling the tilting angle of meta-grating in visible spectra band [102]. Recently, Tang et al. proposed a MEMS mirror based vertical and rotational actuation platform that supports vertical displacement range of 0–4 μm and rotation range of ± 10° [103]. By integrating metasurfaces on this platform, the topological singularities can be effectively tuned, promising for quantum optics applications. Subsequently, it is applied as an adaptive moiré sensor for hyperspectral and hyperpolarimetric imaging [104].

Except electrostatic force, piezoelectric actuator can also support vertical displacement. Piezoelectric actuators provide high precision, low power consumption, and rapid response without pull-in instability, making them suitable for fine tuning of cavity length. In 2021, Meng et al. proposed piezoelectric platform for tunable metasurface [52]. Then, Ding et al. applied this platform to tune non-Hermitian metasurface, realizing the transitions between diabolic points and exceptional points as shown in Fig. 4f [105]. Recently, Wang et al. developed a mode switchable vortex laser based on the same piezoelectric platform [106]. By switching to "on" state, the reflected circular polarized Gaussian laser beam can be converted to vortex laser beam, while it remains as Gaussian beam under "off" state.

In summary, MEMS vertical actuation platform is a powerful tuning platform that provides spatial tunability. As research continues to explore novel physical mechanisms such as bound states in the continuum [107, 108], topological photonics [105], and quantum optics [109], the integration of vertical MEMS actuation with advanced photonic architectures is expected to enable richer tunability and give rise to more exciting and unconventional optical functionalities.

MEMS-enabled reconfigurable metalenses

Metalenses based on planar metasurfaces have emerged as a disruptive optical platform by enabling ultrathin, lightweight, and highly compact alternatives to conventional refractive optics [110–114]. By spatially engineering subwavelength meta-atoms, metalenses can precisely tailor the phase, amplitude, and polarization of incident light, achieving diffraction-limited focusing and

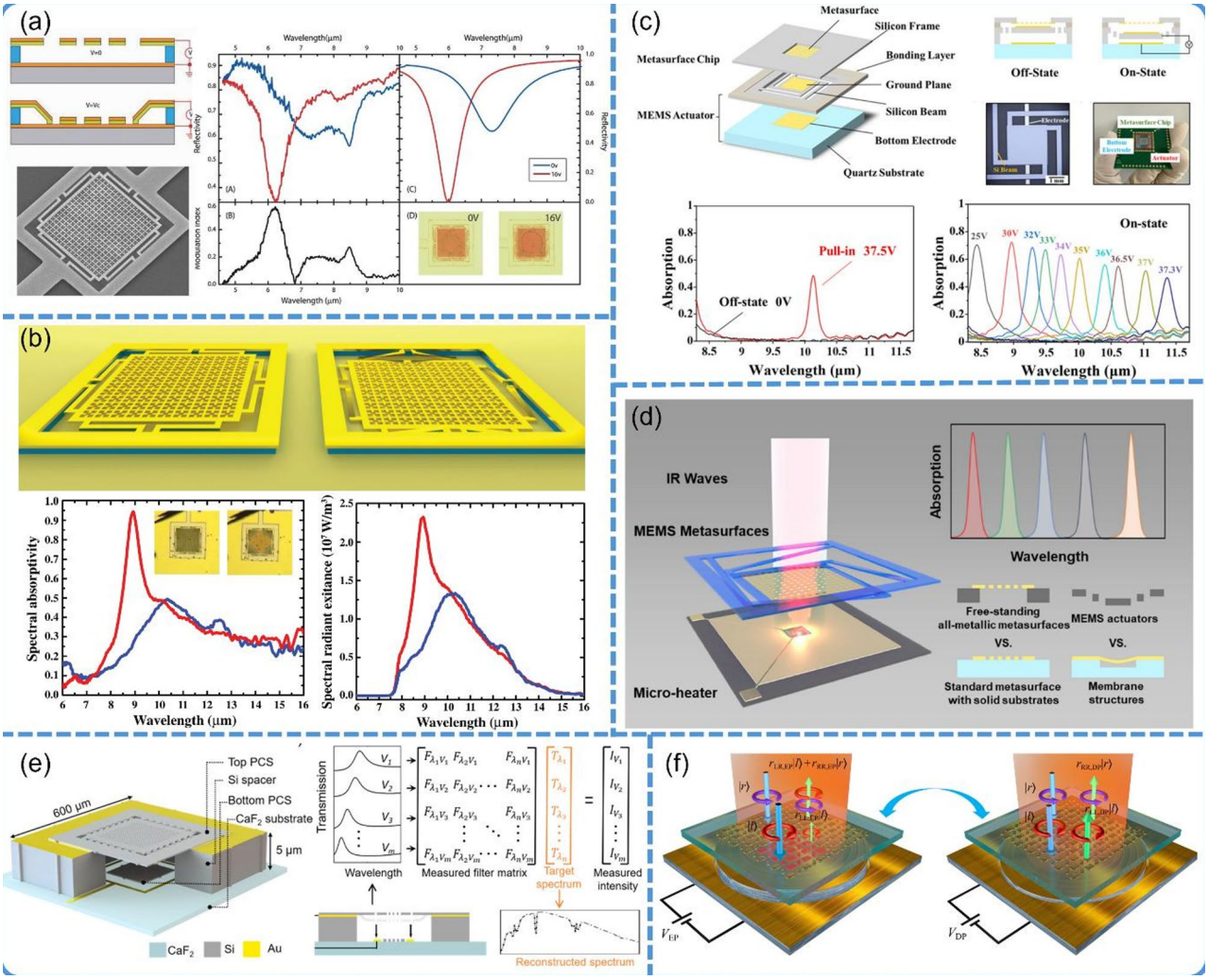

Fig. 4 Micro-nano photonics applications based on MEMS collective vertical actuation of device layer. **a** Tunable mid-infrared absorber and (**b**) tunable metamaterial thermal emitter under room temperature, switched by pull-in effect between metamaterial array and ground reflection mirror. Reproduced with permission [31]. Copyright 2013, Wiley. Reproduced with permission [99]. Copyright 2017, Optica Publishing Group. Continuously tunable MEMS Fabry–Perot cavity actuated by electrostatic force for tunable metamaterials tuned by controlling movement of (**c**) free-standing metallic mirror, **d** free-standing metallic metamaterial layer, and (**e**) freestanding dielectric metamaterial layer. Reproduced with permission [100]. Copyright 2024, American Chemical Society. Reproduced with permission [101]. Copyright 2025, Optica Publishing Group. Reproduced with permission [36]. Copyright 2021, Elsevier. **f** Electrically tunable topological phase transition actuated by piezoelectric reflection mirror. Reproduced with permission [105]. Copyright 2024, AAAS

aberration control within a flat form factor [115]. These unique advantages have stimulated extensive research in imaging [116,117], augmented and virtual reality [118, 119], and compact optical systems [120]. However, similar to other static metasurface devices, conventional metalenses exhibit fixed focal properties once fabricated, which fundamentally limits their adaptability to varying imaging conditions, object distances, and system-level requirements.

To address this limitation, MEMS-enabled reconfigurable metalenses have been proposed to introduce dynamic control over optical focusing through mechanical actuation [121]. Arbabi et al. demonstrated a MEMS-enabled tunable dielectric metasurface doublet lens, in which dynamic focal-length tuning is achieved by mechanically modulating the relative position between the metasurface and the substrate (Fig. 5a) [34]. A displacement of only 1 μm in one metasurface results in a change in optical power exceeding 60 diopters (approximately 4%), with a potential scanning frequency reaching several kilohertz. Moreover, the doublet lens can be integrated with a third metasurface to form a compact microscope with a total thickness of approximately 1 mm, offering a large corrected field of view (~ 500 μm or 40°) and rapid axial scanning capability suitable for three-dimensional imaging. This approach enables continuous focal-length tuning while preserving the high transmission efficiency and low loss inherent to dielectric

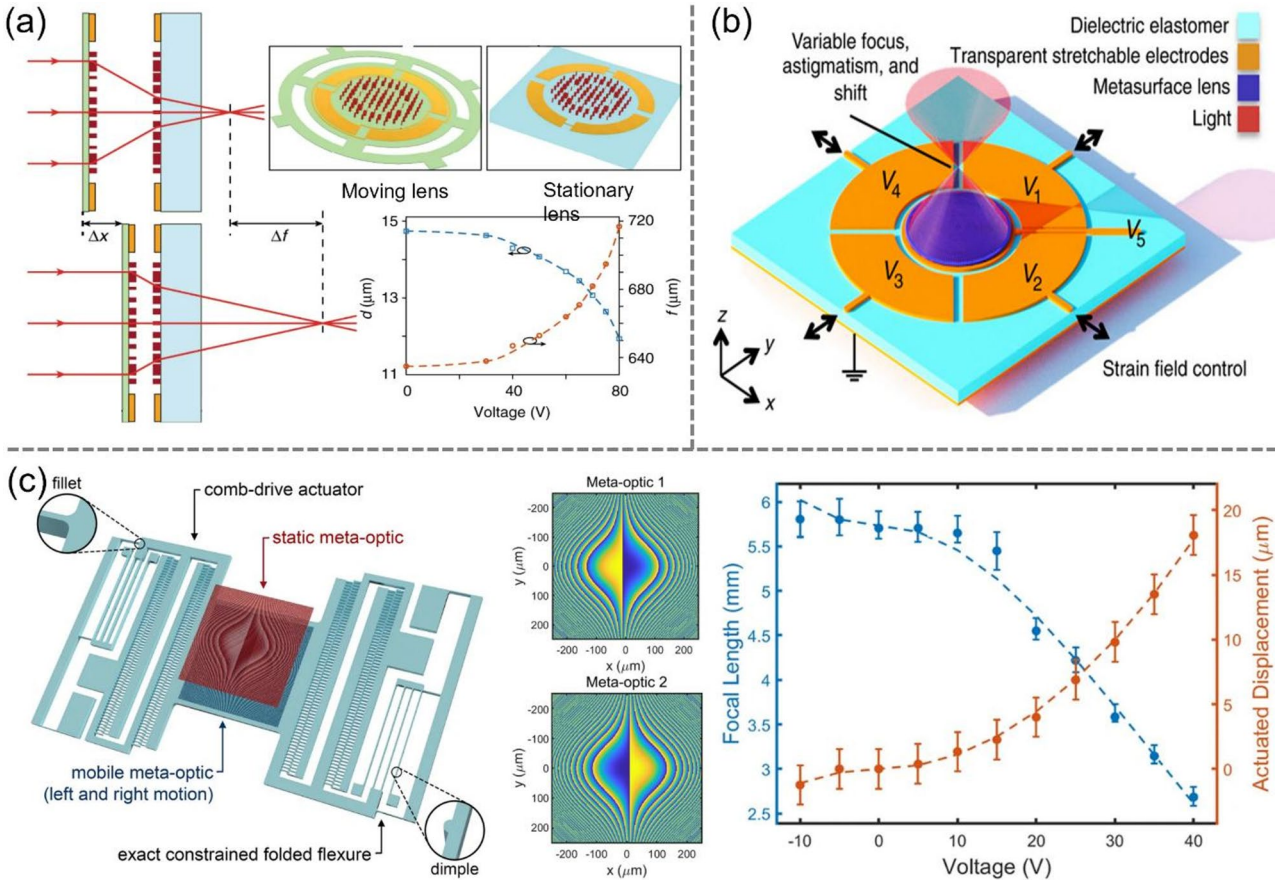

Fig. 5 MEMS-Enabled Reconfigurable Metalenses. **a** Schematic illustration of the tunable doublet and design graphs. Reproduced with permission [34]. Copyright 2018, Springer Nature. **b** Schematic of a metalens integrated with a dielectric elastomer actuator, where five independently addressable electrodes enable programmable control of the metasurface strain field. Reproduced with permission [122]. Copyright 2018, AAAS. **c** MEMS-actuated metasurface Alvarez lens. Reproduced with permission [124]. Copyright 2020, Springer Nature

metasurfaces, without relying on refractive-index modulation or thermal effects. This example highlights the effectiveness of out-of-plane MEMS displacement as a low-power, broadband tuning mechanism for planar optical components.

Beyond simple focal-length tuning, MEMS actuation enables multi-degree-of-freedom control in metasurface-based optical systems. She et al. demonstrated an adaptive metalens capable of simultaneous electrical control over focal length, astigmatism, and lateral focal shift (Fig. 5b) [122]. With a total thickness of only 30 μm, the metalens achieves more than 100% focal-length tuning while providing real-time correction of astigmatism and image shift—functionalities that were previously accessible primarily in electron-optical systems. Such multifunctional control is particularly important for adaptive imaging and optical alignment, where conventional solutions typically rely on bulky and mechanically complex components. This work underscores how MEMS integration transforms metalenses from passive focusing elements into actively controlled optical systems with greatly enhanced versatility.

Another efficient strategy for achieving tunable focusing relies on the Alvarez metalens [123], in which focal-length modulation is realized through lateral displacement of two complementary phase profiles. Han et al. demonstrated a MEMS-actuated metasurface Alvarez lens that enables continuous and rapid focal-length tuning while minimizing optical aberrations (Fig. 5c) [124]. Specifically, under driving voltages below 20 V, a lateral displacement of 6.3 μm yields a focal-length tuning range of 68 μm, corresponding to a tuning amplification factor exceeding ten between the mechanical input and optical output. Compared with out-of-plane actuation schemes, the lateral MEMS displacement employed in Alvarez metalenses offers advantages in mechanical stability, structural compactness, and reduced sensitivity to fabrication imperfections. This approach illustrates how computationally inspired optical design can be synergistically combined with MEMS actuation to achieve large-range tunability using simplified mechanical architectures.

Early demonstrations in this area primarily focused on proof-of-concept devices, whereas more recent studies have shifted toward scalability and large-range tunability with the goal of practical deployment. Han et al. reported MEMS-integrated meta-optical devices fabricated using high-throughput, wafer-compatible processes [125]. The demonstrated devices employ a novel nanofabrication approach that supports larger-aperture meta-optical elements, while flip-chip bonding is used to improve alignment accuracy between the metasurfaces. Notably, the devices adopt an Alvarez lens architecture and achieve a focal-length tuning range of 3.1 mm (corresponding to 200 diopters) under driving voltages below 40 V. By combining metasurface optics with robust MEMS actuators, this work demonstrates large mechanical displacements and correspondingly wide focal-length tuning ranges, while maintaining optical efficiency and device uniformity over large areas. The adoption of scalable manufacturing techniques represents a critical step toward commercialization, addressing long-standing challenges in yield, repeatability, and system-level integration for reconfigurable planar optical devices.

In summary, these works illustrate the rapid evolution of MEMS-enabled reconfigurable metalenses from basic tunable focusing elements to multifunctional, scalable, and application-ready flat optical systems. By leveraging precise mechanical control, MEMS-actuated metalenses overcome the intrinsic rigidity of static metasurfaces and enable adaptive focusing, aberration correction, and system-level reconfigurability. As MEMS fabrication and heterogeneous integration continue to mature, reconfigurable metalenses are poised to play a critical role in next-generation compact imaging systems, wearable optics, and intelligent photonic platforms.

MEMS-enabled reconfigurable terahertz metasurfaces

The integration of MEMS actuation with metamaterial and metasurface resonators has enabled a powerful class of structurally reconfigurable platforms for dynamic control of electromagnetic waves [24, 32, 35, 81, 126–143]. By embedding compliant micro-/nano-mechanical elements directly into subwavelength unit cells, these systems can modulate resonance frequency, linewidth, polarization response, and near-field coupling with high reversibility and device-level scalability. Compared with material-property tuning such as phase-change or carrier injection, MEMS-based reconfiguration offers a geometry-first route that is broadly compatible with lithographic fabrication and can be designed for large range, multi-state programmability. Figure 6 highlights representative MEMS-enabled reconfigurable metamaterial and metasurface platforms that collectively illustrate the evolution from basic spectral tuning to programmable, sensing-oriented, and high-performance nanophotonic functionality.

Early terahertz demonstrations, including electrothermally actuated omega-ring metamaterials (Fig. 6a) [24] and interpixelated SRR/eSRR architectures, established continuous resonance tuning and independently addressable electric and magnetic responses (Fig. 6b) [130]. In parallel, symmetry-preserving multiband cantilever designs showed that reconfiguration could be achieved while maintaining polarization robustness (Fig. 6c) [131]. These early platforms are important not only as historical starting points, but also because they introduced concepts that remain central in modern nanophotonic systems, including geometry-native tunability, multistate operation, and unit-cell-level programmability.

As the field matured, MEMS metasurfaces moved beyond simple frequency shifting toward richer functional behavior. Bidirectional thermomechanical deformation enabled adaptive spectral control over wide environmental conditions, pointing to the relevance of MEMS platforms for filtering and sensing applications in realistic settings (Fig. 6d) [139]. At the same time, mechanically induced structural asymmetry was used to activate sharp Fano resonances and distinct electromagnetic states, allowing MEMS metasurfaces to support multiple-input–output logic operations (Fig. 6e) [32]. These advances are especially relevant from a modern nanophotonic perspective because they connect structural actuation with high-contrast resonant features, near-field localization, and information-processing capability. In other words, MEMS control is not limited to moving a resonance peak; it also enables deliberate engineering of modal coupling, field enhancement, and functional state switching, which are increasingly important in reconfigurable photonic and metasurface-based systems.

More recent developments further bridge THz reconfigurable metasurfaces with broader nanophotonic system functionality. Hybrid platforms combining MEMS tuning with ultrafast optical excitation demonstrated that large spectral agility can coexist with high-speed modulation, illustrating a pathway toward spatiotemporally programmable devices (Fig. 6f) [35]. This trend extends naturally into infrared nanophotonics, where high-Q resonances are highly sensitive to nanoscale mechanical perturbations. A representative example is the electrically driven mirror-coupled quasi-BIC platform in the mid-infrared, in which MEMS control of resonator spacing enabled microsecond response, a tuning span of approximately 400 nm, and a 2.9× enhancement in gas-sensing performance through improved alignment between photonic resonance and molecular absorption (Fig. 6g) [143].

Overall, these milestones illustrate a clear evolution of MEMS -enabled metamaterials from single-mode

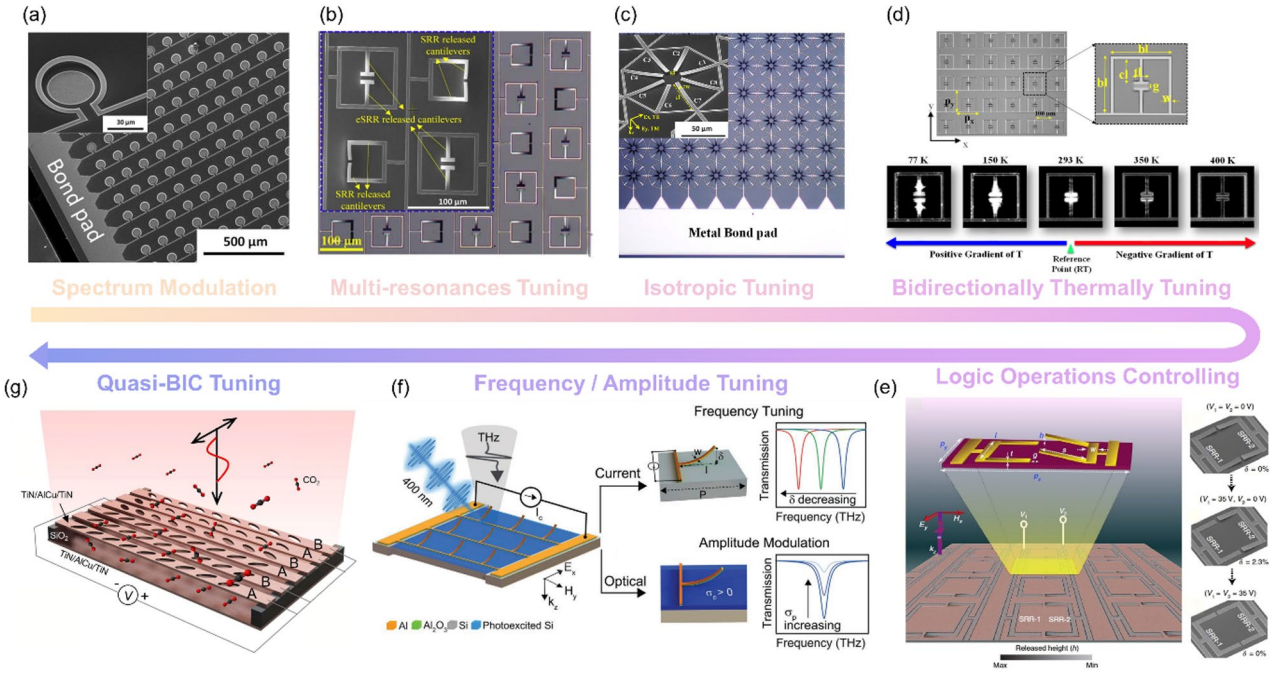

Fig. 6 Timeline and representative functionalities of MEMS/NEMS-enabled tunable metamaterials and metasurfaces. **a** SEM images of an electrothermally actuated omega-ring THz metamaterial array enabling continuous spectral modulation. Reproduced with permission [24]. Copyright 2014, AIP Publishing. **b** Interpixelated MEMS metamaterial integrating SRR/eSRR elements for independently addressable multi-resonance tuning. Reproduced with permission [130]. Copyright 2015, Optica Publishing Group. **c** Rotationally symmetric, multiband MEMS metamaterial with out-of-plane microcantilevers for polarization-insensitive tuning. Reproduced with permission [131]. Copyright 2015, Springer Nature. **d** Bimaterial microcantilever metasurface showing bidirectional thermal actuation and temperature-dependent optical response across cryogenic to elevated temperatures. Reproduced with permission [139]. Copyright 2017, AIP Publishing. **e** Reconfigurable Fano metasurface for digital logic manipulation, where mechanically induced asymmetry enables multi-state control and logic operations. Reproduced with permission [32]. Copyright 2018, Springer Nature. **f** Multi-stimulus spatiotemporal modulation combining MEMS-driven frequency agility (electrical current) with ultrafast optical pumping for amplitude switching. Reproduced with permission [35]. Copyright 2020, Wiley. **g** MEMS-tunable mirror-coupled quasi-BIC nanophotonic platform in the mid-infrared for resonance alignment and enhanced gas sensing. Reproduced with permission [143]. Copyright 2025, IEEE

spectral tuning toward multi-resonant, polarization-robust, and multi-state reconfigurable metasurfaces, and ultimately to high-Q nanophotonic platforms where small mechanical motions enable substantial functional gains. Across the timeline, mechanical actuation provides a uniquely "geometry-native" control knob that is reversible and scalable, allowing designers to engineer not only resonance frequency and amplitude but also higher-level behaviors such as logic-state switching, spatiotemporal modulation, and adaptive sensing. This progression establishes MEMS reconfiguration as a key pathway for realizing programmable electromagnetic devices that bridge unit-cell physics and system-level functions.

AI-assisted design of reconfigurable metasurfaces

Despite the rapid expansion of achievable functions, one bottleneck is the increasing challenge for designing: MEMS metasurfaces combine subwavelength units with mechanically deformable geometries, creating a high-dimensional, strongly coupled parameter space that is difficult to navigate through full-wave simulation and manual intuition. In particular, multi-objective targets require repeated evaluation across many geometries and mechanical states, quickly making conventional optimization prohibitively expensive. These challenges naturally motivate the adoption of deep-learning-assisted design paradigms, where neural networks serve as fast surrogates, inverse designers, and generative engines to accelerate exploration and enable co-design of MEMS structures and electromagnetic responses.

Deep learning (DL) has rapidly become a central tool in computational physics [144–156] as it offers a practical way to learn fast surrogates of expensive numerical solvers, invert the mapping from response to structure, and discover new designs beyond human intuition. In metamaterial/metasurface research, this trend is especially pronounced: subwavelength unit cells yield highly nonlinear spectral responses, and design spaces quickly become high-dimensional once one moves from static patterns to reconfigurable MEMS geometries. As a result, DL is increasingly used not only to speed up full-wave electromagnetic workflows, but also to couple device design with system-level goals.

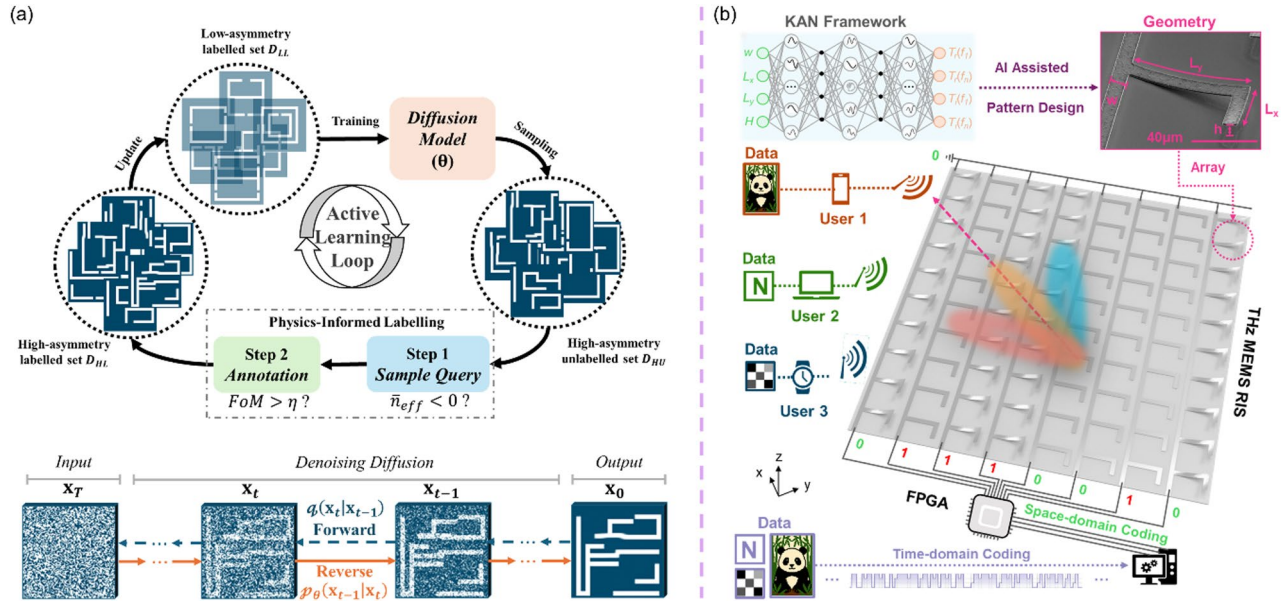

Fig. 7 Deep-learning-assisted MEMS metamaterial/metasurface design frameworks. **a** Diffusion-model-based inverse design pipeline combined with a physics-constrained active-learning loop, where the diffusion generator samples candidate high-asymmetry patterns and a physics-informed labeling/annotation step selects high-performance designs to iteratively update the training set. Reproduced with permission [164]. Copyright 2024, Wiley. **b** KAN-enabled surrogate modeling and AI-assisted design of a THz MEMS reconfigurable intelligent surface (RIS), illustrating geometry-to-response learning, pattern optimization, and subsequent space-/time-domain coding for programmable beam control and information transmission. Reproduced with permission [165]. Copyright 2026, Springer Nature

A common starting point is forward modeling: given geometric/material parameters, predict spectral amplitude/phase (or polarization-dependent scattering parameters). In this setting, parameter-regression multilayer perceptrons (MLP) [157] provide a lightweight baseline, while more expressive alternatives such as Kolmogorov–Arnold Networks (KAN) [158] aim to improve accuracy and generalization by adopting different functional representations. Beyond these "vector-in, spectrum-out" regressors, convolutional neural networks (CNN) [159] are widely used when the geometry is represented as an image grid, since they can extract localized spatial pattern that correlate with resonant features. For capturing long-range couplings and global dependencies, attention-based architectures such as Transformers [160] have emerged as a flexible option. For problems better posed as learning an operator, Fourier Neural Operators (FNO) [161] provide spectral-domain modeling with strong efficiency in representing global smooth components. Finally, for inverse design and exploration, generative models—including VAE [162], GAN [163], and diffusion models [164]—learn a distribution over viable structures and can generate candidate geometries that satisfy desired electromagnetic constraints. These representative architecture families are now widely recognized as a "toolbox" for MEMS metamaterial design.

As displayed in Fig. 7a, Dai et al. proposed a physics-constrained active learning mechanism for MEMS metamaterial design [164]. Their work starts from a small set of known structures and iteratively enriches the dataset by selectively labeling only promising generated candidates. Concretely, a small labeled set of low-asymmetry structures is used to initialize training, after which the diffusion model generates an unlabeled candidate set. A physics-guided screening step then reduces the annotation burden by selecting only structures likely to exhibit terahertz resonance. Samples that exceed a threshold are merged back into training for the next active-learning iteration. In this way, the training distribution gradually shifts toward higher asymmetry and stronger resonance performance, enabling the model to learn beyond the limited initial prior set. The proposed diffusion models provide superior generative stability and can synthesize structural images with higher diversity and quality, which is particularly beneficial for exploring high-degree-of-freedom (high-DoF) MEMS metamaterial patterns.

In Fig. 7b, Wang et al. focuses on the complementary need for fast, accurate forward prediction and efficient geometry optimization for deformable MEMS metasurfaces [165]. They present a CMOS-compatible MEMS-based THz RIS designed through a machine-learning-assisted workflow, and specifically employ KAN to map the deformable L-shaped MEMS meta-atom geometry to its THz transmission amplitude and phase responses. This surrogate then supports rapid design-space exploration and geometry optimization without relying on manual heuristics, allowing the metasurface to be engineered for multi-functional wavefront control and

coding. The fabricated RIS exhibits π-phase switching at 0.6 THz and, when the operating frequency is tuned over 0.3–0.8 THz, achieves beam steering from ± 60° to ± 13.5°. Beyond beam steering, the author demonstrates multi-level amplitude modulation and programmable spatial–temporal coding for directional THz transmission of text, grayscale images, and four-color images, realizing a PSNR exceeding 34 dB. Importantly, this work exemplifies how AI can move beyond unit-cell regression to close the loop between MEMS geometry optimization and system demonstrations, enabling rapid, fabrication-aware design iterations for complicated MEMS metamaterial design.

For vertically actuated MEMS–nanophotonic platforms discussed in Sect. 3.3, AI is especially valuable because the design problem is inherently multi-physics and high-dimensional: the optical response is governed not only by the in-plane metasurface geometry, but also by mechanically tunable cavity spacing, local stiffness distribution, and often non-uniform displacement profiles across the suspended platform. A useful methodological precedent is provided by Guo et al., who developed a deep-learning framework for non-parameterized MEMS structural design in which candidate geometries are represented as topologically unconstrained pixelated binary images and labeled using finite-element simulations [166]. Their trained network could rapidly predict device-relevant physical quantities, screen and rank thousands of design candidates, and achieve orders-of-magnitude acceleration over conventional numerical solvers. In this sense, AI is not merely a post hoc accelerator, but an enabling framework for jointly designing the photonic and mechanical degrees of freedom that underlie vertically reconfigurable nanophotonic devices.

For metalenses mentioned in Sect. 3.4, AI becomes particularly valuable when the design objective extends beyond a single static phase mask to multi-state wavefront engineering. In such cases, the target optical performance depends not only on the meta-atom geometry itself, but also on additional state variables introduced by reconfiguration, such as incident angle, lateral displacement, vertical separation, or strain-induced deformation. A recent example was reported by Wang et al., who developed a hybrid deep-learning framework integrating KAN, MLP, CNN, and Transformer modules to predict the phase and transmission responses of diverse meta-atoms under multiple incident angles with accuracies exceeding 95% [167]. Based on this model, they rapidly generated fabrication-compatible meta-atom libraries and experimentally realized a multi-angle focusing metalens for MEMS LiDAR, which maintained effective focusing from 0° to 30° incidence and reduced the maximum focal shift to only 20 μm, approximately one-tenth that of a conventional metalens with the same size. This work clearly demonstrates how AI can jointly optimize meta-atom geometry and phase-profile design across multiple operating states. In their design process, AI can be used to co-optimize structural geometry together with actuation-dependent phase redistribution, thereby enabling larger focal tuning ranges while suppressing focal drift and aberrations across reconfigured states.

In summary, deep learning is reshaping MEMS metamaterial/metasurface design by addressing two complementary needs: data-efficient discovery and fast, accurate design closure. Together with other emerging architectures, these approaches provide a practical toolbox to manage the coupled electromagnetic–mechanical design space, enabling faster exploration, improved performance targeting, and closer integration between device-level metasurface engineering and system-level functionalities.

Conclusion and outlook

MEMS-enabled reconfigurable metasurface and nanophotonics has rapidly evolved into a versatile and powerful paradigm for dynamic light manipulation, overcoming the intrinsic rigidity of conventional static nanophotonic devices. By introducing mechanical degrees of freedom, MEMS provides low-power, large-range, and broadband tunability, enabling adaptive control over optical resonances, phase profiles, coupling conditions, and radiation characteristics. As reviewed in this article, such capabilities have led to significant advances across a wide range of application domains, including adaptive sensing, tunable metasurface-based radiation sources, reconfigurable silicon photonic platforms, dynamic metalenses, and terahertz metasurfaces.

Despite this progress, several challenges must be addressed to fully realize the potential of MEMS-enabled nanophotonics in practical systems. From an engineering perspective, long-term reliability and packaging remain critical issues for practical deployment. Released MEMS structures are often susceptible to stiction, particularly in devices with small gaps or large movable areas, which can degrade device yield and operational stability. In addition, dielectric charging in electrostatic actuators may lead to drift in actuation voltage and long-term performance degradation. For large-area metasurface platforms, wafer-level encapsulation and hermetic packaging strategies are required to protect fragile nanostructures while maintaining optical access. Mechanical fatigue in repeatedly actuated displacement platforms also becomes increasingly important for applications requiring high cycling stability. Addressing these issues will be essential for translating MEMS-enabled nanophotonics from laboratory demonstrations to robust system-level technologies. Furthermore, from a device design perspective, trade-offs among tuning range, response speed, optical

efficiency, and device footprint require careful co-design of MEMS structures and nanophotonic elements. From a fabrication standpoint, achieving high yield, wafer-scale uniformity, and CMOS compatibility is essential for large-scale deployment and commercialization.

Looking forward, the field is poised to transition from reconfigurable toward programmable and intelligent nanophotonic systems. The integration of artificial intelligence and machine learning offers new opportunities for inverse design, multi-objective optimization, and closed-loop control, enabling devices that can autonomously adapt to changing environments and application requirements. Moreover, tighter integration of MEMS-enabled nanophotonics with detectors, electronics, and on-chip signal processing is expected to facilitate compact, system-level solutions for sensing, imaging, and communication.

With continued advances in MEMS fabrication, heterogeneous integration, and intelligent control, MEMS-enabled reconfigurable metasurface and nanophotonics are expected to play a pivotal role in next-generation adaptive optical systems, bridging the gap between laboratory-scale demonstrations and real-world applications. The convergence of mechanics, photonics, and intelligence will ultimately redefine how optical functionality is designed, controlled, and deployed across diverse technological domains.

Acknowledgements
This research was supported by the Agency for Science, Technology and Research (A*STAR) under Grant Nos. M24W1NS005 and M23M5a0069; the Ministry of Education (MOE) under the research Grant No. R-263-000-F18-112/A-0009520-01-00; the National Research Foundation Singapore under Grant No. CRP28-2022-0038; the MTC Programmatic Funds (Grant No. M22L1b0110); the National Semiconductor Translation and Innovation Centre (Grant No. M24W1NS005); the Reimagine Re-search Scheme (RRSC) Project (Grant Nos. A-0009037-02-00 and A0009037-03-00) at National University of Singapore.

Authors' contributions
D. L., W. L. and Y. W. contributed equally to this work. D. L., W. L., Y. W. and D. Z. wrote the main manuscript text. All authors reviewed the manuscript.

Data availability
No datasets were generated or analysed during the current study.

Declarations

Competing interests
The authors declare no competing interests.

Received: 31 December 2025 / Accepted: 19 March 2026
Published online: 24 March 2026

References

1. Ren H, Maier SA (2023) Nanophotonic Materials for Twisted-Light Manipulation. Adv Mater 35:2106692
2. Koenderink AF, Alù A, Polman A, Nanophotonics (2015) Shrinking light-based technology. Science 348:516–521
3. Tonkaev P, Sinev IS, Rybin MV, Makarov SV, Kivshar Y (2022) Multifunctional and transformative metaphotonics with emerging materials. Chem Rev 122:15414–15449
4. Altug H, Oh SH, Maier SA, Homola J (2022) Advances and applications of nanophotonic biosensors. Nat Nanotechnol 17:5–16
5. Tittl A et al (2018) Imaging-based molecular barcoding with pixelated dielectric metasurfaces. Science 360:1105–1109
6. Rosas S et al (2023) Metasurface-Enhanced Mid-Infrared Spectrochemical Imaging of Tissues. Adv Mater 35:e2301208
7. Zhou H et al (2024) Surface plasmons-phonons for mid-infrared hyperspectral imaging. Sci Adv 10:eado3179
8. Zhang L et al (2024) Real-time machine learning–enhanced hyperspectropolarimetric imaging via an encoding metasurface. Sci Adv 10:eadp5192
9. To Ys et al (2025) Phase Change Material-Driven Tunable Metasurface for Adaptive Terahertz Sensing and Communication in 6G Perceptive Networks. Adv Funct Mater 36:e15085
10. Zhou H, Li D, Lv Q, Lee C (2025) Integrative plasmonics: optical multi-effects and acousto-electric-thermal fusion for biosensing, energy conversion, and photonic circuits. Chem Soc Rev 54:5342–5432
11. Fan K, Averitt RD, Padilla W (2022) Active and tunable nanophotonic metamaterials. Nanophotonics 11:3769–3803
12. Zograf GP, Petrov MI, Makarov SV, Kivshar YS (2021) All-dielectric thermonanophotonics. Adv Opt Photonics 13:643–702
13. Wuttig M, Bhaskaran H, Taubner T (2017) Phase-change materials for non-volatile photonic applications. Nat Photonics 11:465–476
14. Dong W et al (2018) Tunable mid-infrared phase-change metasurface. Adv Opt Mater 6:1701346
15. Wang Q et al (2016) Optically reconfigurable metasurfaces and photonic devices based on phase change materials. Nat Photonics 10:60–65
16. Haffner C et al (2019) Nano–opto-electro-mechanical switches operated at CMOS-level voltages. Science 366:860–864
17. Liu W, Xu S, Lee C (2025) Ultracompact on-chip spectral shaping using pixelated nano-opto-electro-mechanical gratings. Science 389:806–810
18. Wang Z et al (2024) Two-dimensional materials for tunable and nonlinear metaoptics. Adv Photonics 6:034001–034001
19. Zheng Z, Huang Y, Wu F, Zhang H, Fang Z (2023) Multidimensional modulation of light fields via a combination of two-dimensional materials and metastructures. Sci China Inform Sci 66:160403
20. Kang L, Jenkins RP, Werner DH (2019) Recent progress in active optical metasurfaces. Adv Opt Mater 7:1801813
21. Ding F, Meng C, Bozhevolnyi S (2024) I. Electrically tunable optical metasurfaces. Photonics Insights 3:R07–R07
22. Jung C, Lee E, Rho J (2024) The rise of electrically tunable metasurfaces. Sci Adv 10:eado8964
23. Uenishi Y, Tsugai M, Mehregany M (1995) Micro-opto-mechanical devices fabricated by anisotropic etching of (110) silicon. J Micromechanics Microengineering 5:305
24. Ho CP et al (2014) Electrothermally actuated microelectromechanical systems based omega-ring terahertz metamaterial with polarization dependent characteristics. Appl Phys Lett 104:161104
25. Gyger S et al (2021) Reconfigurable photonics with on-chip single-photon detectors. Nat Commun 12:1408
26. Xu A et al (2026) Transducers Across Scales and Frequencies: A System-Level Framework for Multiphysics Integration and Co-Design. Adv Mater Technol 0:e02093
27. Hu Y-Q et al (2025) Artificial Intelligence in Nanophotonics: From Design to Optical Computing. Chin Phys Lett 42:080802
28. Zhou H, Li D, Lee C (2025) Technology landscape review of in-sensor photonic intelligence: from optical sensors to smart devices. AI Sens 1:5
29. Singh J et al (2007) A two axes scanning SOI MEMS micromirror for endoscopic bioimaging. J Micromechanics Microengineering 18:025001
30. Ma F et al (2013) Polarization-sensitive microelectromechanical systems based tunable terahertz metamaterials using three dimensional electric split-ring resonator arrays. Appl Phys Lett 102:161912
31. Liu X, Padilla WJ (2013) Dynamic Manipulation of Infrared Radiation with MEMS Metamaterials. Adv Opt Mater 1:559–562
32. Manjappa M et al (2018) Reconfigurable MEMS Fano metasurfaces with multiple-input–output states for logic operations at terahertz frequencies. Nat Commun 9:4056
33. Seok TJ, Quack N, Han S, Muller RS, Wu MC (2016) Large-scale broadband digital silicon photonic switches with vertical adiabatic couplers. Optica 3:64–70

34. Arbabi E et al (2018) MEMS-tunable dielectric metasurface lens. Nat Commun 9:812
35. Pitchappa P et al (2020) Frequency-agile temporal terahertz metamaterials. Adv Opt Mater 8:2000101
36. Chang Y et al (2021) Development of triboelectric-enabled tunable Fabry-Pérot photonic-crystal-slab filter towards wearable mid-infrared computational spectrometer. Nano Energy 89:106446
37. Li K, Liang Y, Liu Y, Lin Y-S (2025) Tunable MEMS-based meta-absorbers for nondispersive infrared gas sensing applications. Microsystems Nanoengineering 11:2
38. Gu T, Kim HJ, Rivero-Baleine C, Hu J (2023) Reconfigurable metasurfaces towards commercial success. Nat Photonics 17:48–58
39. Zhao Y et al (2024) Mechanically reconfigurable metasurfaces: fabrications and applications. npj Nanophotonics 1:16
40. Zheludev NI, Kivshar YS (2012) From metamaterials to metadevices. Nat Mater 11:917–924
41. Ou JY, Plum E, Zhang J (2013) Zheludev, N. I. An electromechanically reconfigurable plasmonic metamaterial operating in the near-infrared. Nat Nanotechnol 8:252–255
42. Guo X et al (2025) Advances in Intelligent Nano-Micro-Scale Sensors and Actuators: Moving toward Self-Sustained Edge AI Microsystems. Adv Mater 37:e10417
43. Zhao X, Duan G, Li A, Chen C, Zhang X (2019) Integrating microsystems with metamaterials towards metadevices. Microsystems nanoengineering 5:5
44. Martyniuk M et al (2022) Optical microelectromechanical systems technologies for spectrally adaptive sensing and imaging. Adv Funct Mater 32:2103153
45. Shaltout AM, Shalaev VM, Brongersma ML (2019) Spatiotemporal light control with active metasurfaces. Science 364:eaat3100
46. Wang Z et al (2026) Terahertz MEMS actuators and applications. Microsystems Nanoengineering 12:69
47. Timoshenko S (1925) Analysis of bi-metal thermostats. J Opt Soc Am 11:233–255
48. Senturia SD (2001) Microsystem design. Boston, MA, Springer US. https://doi.org/10.1007/b117574
49. Liu C (2012) Foundations of MEMS, 2nd edn. Pearson Education, Upper Saddle River, NJ
50. Potekhina A, Wang C Review of electrothermal actuators and applications. Actuators 8:69
51. Elata D, Bamberger H (2006) On the dynamic pull-in of electrostatic actuators with multiple degrees of freedom and multiple voltage sources. J Microelectromech Syst 15:131–140
52. Meng C et al (2021) Dynamic piezoelectric MEMS-based optical metasurfaces. Sci Adv 7:eabg5639
53. Qiao L et al (2024) Designing transparent piezoelectric metasurfaces for adaptive optics. Nat Commun 15:805
54. Dirdal CA et al (2022) MEMS-tunable dielectric metasurface lens using thin-film PZT for large displacements at low voltages. 47:1049–1052
55. Smits JG, Dalke SI, Cooney TK (1991) The constituent equations of piezoelectric bimorphs. Sens actuators A: Phys 28:41–61
56. Li D, Wu X, Chen Z, Liu T, Mu X (2025) Surface-enhanced spectroscopy technology based on metamaterials. Microsystems Nanoengineering 11:60
57. Li D, Zhou H, Ren Z, Lee C (2025) Advances in MEMS, optical MEMS, and nanophotonics technologies for volatile organic compound detection and applications. Small Sci 5:2400250
58. Li D, Xu C, Xie J, Lee C (2023) Research progress in surface-enhanced infrared absorption spectroscopy: from performance optimization, sensing applications, to system integration. Nanomaterials 13:2377
59. Kim I et al (2024) Ultrafast Metaphotonic PCR Chip with Near-Perfect Absorber. Adv Mater 36:e2311931
60. Kim I et al (2023) Metasurfaces-Driven Hyperspectral Imaging via Multiplexed Plasmonic Resonance Energy Transfer. Adv Mater 35:e2300229
61. Xu C et al (2025) Unraveling the Far-Field Coupling of Multilayered Chiral Metamaterials for CMOS-Enabled Midinfrared Imaging. ACS Nano 19:30292–30302
62. Li D et al (2023) Ultrasensitive Molecular Fingerprint Retrieval Using Strongly Detuned Overcoupled Plasmonic Nanoantennas. Adv Mater 35:e2301787
63. Li D, Zhou H, Ren Z, Xu C, Lee C (2024) Tailoring Light–Matter Interactions in Overcoupled Resonator for Biomolecule Recognition and Detection. Nano-Micro Lett 17:1–19
64. Li D, Zhou H, Hui X, He X, Mu X (2021) Plasmonic Biosensor Augmented by a Genetic Algorithm for Ultra-Rapid, Label-Free, and Multi-Functional Detection of COVID-19. Anal Chem 93:9437–9444
65. Li D et al (2021) Multifunctional Chemical Sensing Platform Based on Dual-Resonant Infrared Plasmonic Perfect Absorber for On-Chip Detection of Poly(ethyl cyanoacrylate). Adv Sci 8:2101879
66. Hui X et al (2021) Infrared Plasmonic Biosensor with Tetrahedral DNA Nanostructure as Carriers for Label-Free and Ultrasensitive Detection of miR-155. Adv Sci 8:e2100583
67. Zhou H et al (2020) Metal-Organic Framework-Surface-Enhanced Infrared Absorption Platform Enables Simultaneous On-Chip Sensing of Greenhouse Gases. Adv Sci 7:2001173
68. Wang R et al (2025) Multifunctional Terahertz Biodetection Enabled by Resonant Metasurfaces. Adv Mater, 37:e2418147
69. Wang R et al (2025) Ultra-compact broadband terahertz spectroscopy sensor enabled by resonant-gradient metasurface. Nat Commun 16:11462
70. Zhou H, Li D, Ren Z, Mu X, Lee C (2022) Loss-induced phase transition in mid-infrared plasmonic metamaterials for ultrasensitive vibrational spectroscopy. *InfoMat* 4(12): e12349
71. Li D et al (2026) Artificial Intelligence-Integrated Overcoupled Resonator for Multifunctional Pesticide Spectral Classification and Quantification. ACS Nano 20:7730–7742
72. Chen Z, Li D, Zhou H, Liu T, Mu X (2023) A hybrid graphene metamaterial absorber for enhanced modulation and molecular fingerprint retrieval. Nanoscale 15:14100–14108
73. Xu C et al (2023) Near-Field Coupling Induced Less Chiral Responses in Chiral Metamaterials for Surface-Enhanced Vibrational Circular Dichroism. Adv Funct Mater 34:2314482
74. Neubrech F, Huck C, Weber K, Pucci A, Giessen H (2017) Surface-Enhanced Infrared Spectroscopy Using Resonant Nanoantennas. Chem Rev 117:5110–5145
75. Wei J et al (2019) Ultrasensitive Transmissive Infrared Spectroscopy via Loss Engineering of Metallic Nanoantennas for Compact Devices. ACS Appl Mater Inter 11:47270–47278
76. Ren Z, Zhang Z, Wei J, Dong B, Lee C (2022) Wavelength-multiplexed hook nanoantennas for machine learning enabled mid-infrared spectroscopy. Nat Commun 13:3859
77. Chang Y et al (2018) All-Dielectric Surface-Enhanced Infrared Absorption-Based Gas Sensor Using Guided Resonance. ACS Appl Mater Interfaces 10:38272–38279
78. Richter FU et al (2024) Gradient High-Q Dielectric Metasurfaces for Broadband Sensing and Control of Vibrational Light-Matter Coupling. Adv Mater 36:e2314279
79. Aigner A, Weber T, Wester A, Maier SA, Tittl A (2024) Continuous spectral and coupling-strength encoding with dual-gradient metasurfaces. Nat Nanotechnol 19:1804–1812
80. Yesilkoy F et al (2019) Ultrasensitive hyperspectral imaging and biodetection enabled by dielectric metasurfaces. Nat Photonics 13:390–396
81. Lin Y-S, Lee C (2014) Tuning characteristics of mirrorlike T-shape terahertz metamaterial using out-of-plane actuated cantilevers. Appl Phys Lett 104:251914
82. Xiao Z et al (2023) Recent Progress in Silicon-Based Photonic Integrated Circuits and Emerging Applications. Adv Opt Mater 11:2301028
83. Cheng Q, Bahadori M, Glick M, Rumley S, Bergman K (2018) Recent advances in optical technologies for data centers: a review. Optica 5:1354–1370
84. Reed GT, Mashanovich G, Gardes FY, Thomson D (2010) Silicon optical modulators. Nat Photonics 4:518–526
85. Midolo L, Schliesser A, Fiore A (2018) Nano-opto-electro-mechanical systems. Nat Nanotechnol 13:11–18
86. Errando-Herranz C et al (2019) MEMS for photonic integrated circuits. IEEE J Sel Top Quantum Electron 26:1–16
87. Pérez D et al (2017) Multipurpose silicon photonics signal processor core. Nat Commun 8:636
88. Kim DU et al (2023) Programmable photonic arrays based on microelectromechanical elements with femtowatt-level standby power consumption. Nat Photonics 17:1089–1096
89. Qiao Q et al (2020) Multifunctional mid-infrared photonic switch using a MEMS-based tunable waveguide coupler. Opt Lett 45:5620–5623
90. Sun H, Qiao Q, Xia J, Lee C, Zhou G (2022) Mid-infrared silicon photonic phase shifter based on microelectromechanical system. Opt Lett 47:5801–5803
91. Qiao Q et al (2022) MEMS-enabled on-chip computational mid-infrared spectrometer using silicon photonics. Acs Photonics 9:2367–2377

92. Liu W et al (2022) Larger-than-unity external optical field confinement enabled by metamaterial-assisted comb waveguide for ultrasensitive long-wave infrared gas spectroscopy. Nano Lett 22:6112–6120
93. Liu WX et al (2021) Suspended silicon waveguide platform with subwavelength grating metamaterial cladding for long-wave infrared sensing applications. Nanophotonics 10:1861–1870
94. Sun H, Qiao Q, Lee C, Zhou G (2025) MEMS-enabled Ultralow Power Consumption Programmable Arbitrary Order Mode Switch. Laser Photonics Reviews 19:2400641
95. Chollet F (2016) Devices based on co-integrated MEMS actuators and optical waveguide: a review. Micromachines 7:18
96. Quack N et al (2023) Integrated silicon photonic MEMS. Microsystems Nanoengineering 9:27
97. Landy NI, Sajuyigbe S, Mock JJ, Smith DR, Padilla WJ (2008) Perfect metamaterial absorber. Phys Rev Lett 100:207402
98. Hasan D, Lee C (2018) Hybrid Metamaterial Absorber Platform for Sensing of CO2 Gas at Mid-IR. Adv Sci 5:1700581
99. Liu XY, Padilla WJ (2017) Reconfigurable room temperature metamaterial infrared emitter. Optica 4:430–433
100. Wang X et al (2024) Micromachined Tunable High-Q Infrared Absorbers Enabled by Free-Standing All-Metallic Metasurfaces. ACS Photonics 11:3870–3877
101. Wang X et al (2025) Design and fabrication method of the MEMS tunable metasurface thermal emitter with free-standing structures. Photonics Res 14:297–308
102. Holsteen AL, Cihan AF, Brongersma ML (2019) Temporal color mixing and dynamic beam shaping with silicon metasurfaces. Science 365:257–260
103. Tang H et al (2024) On-chip multi-degree-of-freedom control of two-dimensional materials. Nature 632:1038–1044
104. Tang H et al (2025) An adaptive moiré sensor for spectro-polarimetric hyperimaging. Nat Photonics 19:463–470
105. Ding F, Deng Y, Meng C, Thrane PC, Bozhevolnyi S (2024) I. Electrically tunable topological phase transition in non-Hermitian optical MEMS metasurfaces. Sci Adv 10:eadl4661
106. Wang C et al (2024) MEMS-metasurface–enabled mode-switchable vortex lasers. Sci Adv 10:eadq6299
107. Sun K, Cai Y, Huang L, Han Z (2024) Ultra-narrowband and rainbow-free mid-infrared thermal emitters enabled by a flat band design in distorted photonic lattices. Nat Commun 15:4019
108. Gromyko D, Loh JS, Feng J, Qiu C-W, Wu L (2025) Enabling all-to-circular polarization up-conversion by nonlinear chiral metasurfaces with rotational symmetry. Phys Rev Lett 134:023804
109. Zhou H et al (2025) Control of chirality and directionality of nonlinear metasurface light source via moiré engineering. Phys Rev Lett 134:043801
110. Khonina SN, Butt MA, Kazanskiy NL (2024) A review on reconfigurable metalenses revolutionizing flat optics. Adv Opt Mater 12:2302794
111. Khorasaninejad M, Capasso F, Metalenses (2017) Versatile multifunctional photonic components. Science 358:eaam8100
112. Tseng ML et al (2018) Metalenses: advances and applications. Adv Opt Mater 6:1800554
113. Kim J et al (2023) Scalable manufacturing of high-index atomic layer-polymer hybrid metasurfaces for metaphotonics in the visible. Nat Mater 22:474–481
114. Yoon G, Kim K, Huh D, Lee H, Rho J (2020) Single-step manufacturing of hierarchical dielectric metalens in the visible. Nat Commun 11:2268
115. Arbabi A, Faraon A (2022) Advances in optical metalenses. Nat Photonics 17:16–25
116. Peng Y et al (2024) Metalens in improving imaging quality: advancements, challenges, and prospects for future display. Laser Photonics Reviews 18:2300731
117. Kim J et al (2026) Electrically Reconfigurable Illumination-Engineering Metalens Enabling Quasi-Dark-Field Biological Imaging. ACS Nano 20:5228–5237
118. Li Y et al (2022) Ultracompact multifunctional metalens visor for augmented reality displays. PhotoniX 3:29
119. Li Z et al (2021) Meta-optics achieves RGB-achromatic focusing for virtual reality. Sci Adv 7:eabe4458
120. Li Z et al (2021) Compact metalens-based integrated imaging devices for near-infrared microscopy. Opt Express 29:27041–27047
121. Roy T et al (2018) Dynamic metasurface lens based on MEMS technology. APL Photonics 3:021302
122. She A, Zhang S, Shian S, Clarke DR, Capasso F (2018) Adaptive metalenses with simultaneous electrical control of focal length, astigmatism, and shift. Sci Adv 4:eaap9957
123. Lohmann AW (1970) A new class of varifocal lenses. Appl Opt 9:1669–1671
124. Han Z, Colburn S, Majumdar A, Böhringer K (2020) F. MEMS-actuated metasurface Alvarez lens. Microsystems nanoengineering 6:79
125. Han Z, Colburn S, Majumdar A, Böhringer KF (2022) Millimeter-scale focal length tuning with MEMS-integrated meta-optics employing high-throughput fabrication. Sci Rep 12:5385
126. Pitchappa P et al (2014) Micro-electro-mechanically tunable metamaterial with enhanced electro-optic performance. Appl Phys Lett 104:151104
127. Ma F, Lin Y-S, Zhang X, Lee C (2014) Tunable multiband terahertz metamaterials using a reconfigurable electric split-ring resonator array. Light: Sci Appl 3:e171–e171
128. Lin YS, Huang CY, Lee C (2015) Reconfiguration of Resonance Characteristics for Terahertz U-Shape Metamaterial Using MEMS Mechanism. IEEE J Sel Top Quantum Electron 21:93–99
129. Pitchappa P et al (2015) Periodic array of subwavelength MEMS cantilevers for dynamic manipulation of terahertz waves. J Microelectromech Syst 24:525–527
130. Pitchappa P, Ho CP, Dhakar L, Lee C (2015) Microelectromechanically reconfigurable interpixelated metamaterial for independent tuning of multiple resonances at terahertz spectral region. Optica 2:571–578
131. Pitchappa P et al (2015) Microelectromechanically tunable multiband metamaterial with preserved isotropy. Sci Rep 5:11678
132. Pitchappa P et al (2016) Active control of near-field coupling in conductively coupled microelectromechanical system metamaterial devices. Appl Phys Lett 108:111102
133. Pitchappa P et al (2016) Reconfigurable Digital Metamaterial for Dynamic Switching of Terahertz Anisotropy. Adv Opt Mater 4:391–398
134. Pitchappa P et al (2016) Active control of electromagnetically induced transparency with dual dark mode excitation pathways using MEMS based tri-atomic metamolecules. Appl Phys Lett 109:211103
135. Ho CP, Pitchappa P, Lee C (2016) Digitally reconfigurable binary coded terahertz metamaterial with output analogous to NOR and AND. J Appl Phys 119:153104
136. Pitchappa P et al (2016) Active Control of Electromagnetically Induced Transparency Analog in Terahertz MEMS Metamaterial. Adv Opt Mater 4:541–547
137. Cong L et al (2017) Active Multifunctional Microelectromechanical System Metadevices: Applications in Polarization Control, Wavefront Deflection, and Holograms. Adv Opt Mater 5:1600716
138. Cong L, Pitchappa P, Lee C, Singh R (2017) Active Phase Transition via Loss Engineering in a Terahertz MEMS Metamaterial. Adv Mater 29:1700733
139. Pitchappa P et al (2017) Bidirectional reconfiguration and thermal tuning of microcantilever metamaterial device operating from 77 K to 400 K. Appl Phys Lett 111:261101
140. Manjappa M, Pitchappa P, Wang N, Lee C, Singh R (2018) Active Control of Resonant Cloaking in a Terahertz MEMS Metamaterial. Adv Opt Mater 6:1800141
141. Pitchappa P, Kumar A, Singh R, Lee C, Wang N (2021) Terahertz MEMS metadevices. J Micromech Microeng 31:113001
142. Xu C, Ren Z, Wei J, Lee C (2022) Reconfigurable terahertz metamaterials: From fundamental principles to advanced 6G applications. iScience 25:103799
143. Zhou H et al MEMS-Driven Electrically Reconfigurable Platform for Photonic Quasi-Bound States in the Continuum. (2025) *23rd International Conference on Solid-State Sensors, Actuators and Microsystems (Transducers)*. Orlando, FL, USA, pp 108–111 (IEEE)
144. Qi S et al (2020) Two-dimensional electromagnetic solver based on deep learning technique. IEEE J Multiscale Multiphysics Comput Techniques 5:83–88
145. Li Y et al (2020) Predicting scattering from complex nano-structures via deep learning. IEEE Access 8:139983–139993
146. Wang Y, Zhou J, Ren Q, Li Y, Su (2021) D. 3-D steady heat conduction solver via deep learning. IEEE J Multiscale Multiphysics Comput Techniques 6:100–108
147. Wang Y, Ren Q (2022) A versatile inversion approach for space/temperature/time-related thermal conductivity via deep learning. Int J Heat Mass Transf 186:122444
148. Wang Y, Wang N, Ren Q (2022) Predicting surface heat flux on complex systems via Conv-LSTM. Case Stud Therm Eng 33:101927
149. Ren Q, Wang Y, Li Y, Qi S (2022) Sophisticated electromagnetic forward scattering solver via deep learning. Springer
150. Wang Y, Ren Q (2023) Deep learning-based forward modeling and inversion techniques for computational physics problems. CRC Press, Boca Raton, FL

151. Wang Y, Gao H, Ren Q (2022) Differential operator approximation based tightly coupled multiphysics solver using cascaded fourier network. Adv Theory Simulations 5:2200409
152. Wang Y, Ren Q Sophisticated electromagnetic scattering solver based on deep learning. (2021) *2021 International Applied Computational Electromagnetics Society Symposium (ACES),* Nanjing, China, pp 1–3 (IEEE)
153. Wang Y, Zhang S (2024) Multi-receptive-field physics-informed neural network for complex electromagnetic media. Opt Mater Express 14:2740–2754
154. Sun X, Du B, Wang Y, Ren Q (2024) Coupled multiphysics solver for irregular regions based on graph neural network. Int J Thermofluids 23:100726
155. Wang Y (2024) Deep multiphysics fields solver established on operator learning transformer and finite element method. IEEE J Multiscale Multiphysics Comput Techniques 9:341–352
156. Gao H et al (2024) Deep learning based time-domain inversion for high-contrast scatterers. J Electromagn Waves Appl 38:1844–1867
157. Peurifoy J et al (2018) Nanophotonic particle simulation and inverse design using artificial neural networks. Sci Adv 4:eaar4206
158. Liu Z et al (2024) Kan: Kolmogorov-arnold networks. arXiv preprint arXiv:2404.19756
159. Jia Y et al (2023) A knowledge-inherited learning for intelligent metasurface design and assembly. Light: Sci Appl 12:82
160. Liao J et al (2025) GLSaT: a spectral-aware transformer-based network enabling highly efficient and precise inverse design in metasurface optical filters. Adv Photonics Nexus 4:056014–056014
161. Augenstein Y, Repan T, Rockstuhl C (2023) Neural operator-based surrogate solver for free-form electromagnetic inverse design. ACS Photonics 10:1547–1557
162. Ma W, Cheng F, Xu Y, Wen Q, Liu Y (2019) Probabilistic representation and inverse design of metamaterials based on a deep generative model with semi-supervised learning strategy. Adv Mater 31:1901111
163. Liu Z, Zhu D, Rodrigues SP, Lee K-T, Cai W (2018) Generative model for the inverse design of metasurfaces. Nano Lett 18:6570–6576
164. Dai Q et al (2025) High-Asymmetry Metasurface: A New Solution for Terahertz Resonance via Active Learning-Augmented Diffusion Model. Adv Sci 13:e08610
165. Wang Y et al (2026) Machine Learning Enabled MEMS Reconfigurable Intelligent Surface for Terahertz Beam Steering and Wireless Communication. 2026 IEEE 39th International Conference on Micro Electro Mechanical Systems (MEMS), Salzburg, Austria, pp 1460–1463 (IEEE)
166. Guo R et al (2022) Deep learning for non-parameterized MEMS structural design. Microsyst Nanoeng 8:91
167. Wang Y et al (2025) Multi-angle focusing metalens designed via KAN deep learning for expanding the reception field of MEMS LiDAR. ACS Photonics 12:3245–3255

Publisher's Note